


Politecnico di Torino


## Politecnico di Torino

Master's Degree in Biomedical Engineering

Academic Year 2025/2026

Graduation Session September 2026


# Validation of an inertial infrared wearable system for stride width estimation in post-stroke and Parkinson's disease cohorts during walking


Supervisors:

Prof. Ing. Andrea Cereatti

Dr. Ing. Rachele Rossanigo

Dr. Ing. Marco Caruso

Candidate:

Thea Salamone

*Ne malum quidem me vicit.*

# Acknowledgements

I would like to sincerely thank Prof. Cereatti for giving me the opportunity to undertake this thesis within his research group, and for his guidance throughout this work.

---

I would also like to thank Marco for his valuable contribution to the development of the project and for accompanying me through its different stages.

---

My deepest and most heartfelt thanks go to Rachele for her constant support, availability, and patience, and for always being there whenever I needed help. I am truly grateful for everything she has done for me.

---

Finally, I am grateful to the entire Cereatti research group, including researchers, PhD students, and fellow thesis students, for enriching this experience and for sharing this part of my academic journey with me.

# Table of Contents

**List of Figures** V

**List of Tables** VII

**List of Abbreviations** VIII

**1 Introduction** 1
- 1.1 Context and motivation . . . 1
- 1.2 Research gap and objectives . . . 2

**2 State of the art** 4
- 2.1 Human gait and spatiotemporal parameters . . . 4
  - 2.1.1 The gait cycle . . . 4
  - 2.1.2 Main spatiotemporal gait parameters . . . 6
- 2.2 Gait impairments in neurological populations . . . 9
  - 2.2.1 Post-stroke gait impairments . . . 9
  - 2.2.2 Gait impairments in Parkinson's disease . . . 10
- 2.3 Instrumented and wearable systems for gait analysis . . . 12
  - 2.3.1 Laboratory-based systems . . . 13
  - 2.3.2 Wearable sensing technologies . . . 18
    - Magneto-inertial sensing . . . 18
    - Pressure insoles . . . 25
    - Infrared time-of-flight distance sensors . . . 27
    - Multi-sensor integration . . . 29

**3 Materials and methods** 30
- 3.1 Participants and clinical characterization . . . 30
- 3.2 Experimental instrumentation . . . 32
  - 3.2.1 INDIP wearable system . . . 32
  - 3.2.2 Stereophotogrammetric reference system . . . 35
- 3.3 Experimental protocol . . . 38

3.3.1 Preliminary acquisitions . . . . . 38
3.3.2 Straight walking . . . . . 39
3.3.3 Two-Minutes Walking Test . . . . . 41
3.4 Data processing and stride-width estimation . . . . . 41
3.4.1 Calibration and data personalisation . . . . . 41
Standard distance-based calibration . . . . . 43
Alternative marker-based calibration . . . . . 44
3.4.2 Wearable stride-width estimation . . . . . 46
3.4.3 Stereophotogrammetric reference stride width . . . . . 49
3.4.4 Matching and validity criteria . . . . . 51
3.5 Statistical analysis . . . . . 52

**4 Results** 54
4.1 Dataset overview . . . . . 54
4.2 Gait characteristics across populations and walking conditions . . . 55
4.3 Stride-width estimation performance . . . . . 57
4.4 Association between wearable and reference stride-width estimates . 60
4.5 Participant-reported acceptability . . . . . 63
4.6 Exploratory analysis of freezing of gait . . . . . 64

**5 Discussion** 67
5.1 Validation across populations and walking conditions . . . . . 67
5.2 Agreement, within-subject tracking and clinical interpretation . . . 69
5.3 Practical applicability and additional potential of the wearable system 72
5.4 Strengths, limitations and future developments . . . . . 73

**6 Conclusions** 76

**Bibliography** 78

# List of Figures


2.1 Schematic representation of step and stride during walking . . . . . 4
2.2 Main phases and functional subphases of the gait cycle . . . . . 5
2.3 Schematic representation of the main spatial gait parameters . . . . 7
2.4 Schematic comparison of gait characteristics . . . . . 9
2.5 Schematic representation of the main manifestations of freezing of gait 12
2.6 Typical configuration of an instrumented gait-analysis laboratory . 14
2.7 Principle of three-dimensional marker reconstruction in a stereophotogrammetric system . . . . . 15
2.8 Schematic representation of an anatomical calibration . . . . . 16
2.9 Schematic representation of soft-tissue artefact in marker-based motion analysis. . . . . 17
2.10 Typical architecture of a wearable magneto-inertial measurement unit 19
2.11 Schematic representation of one sensing axis of a capacitive MEMS accelerometer . . . . . 20
2.12 Schematic representation of the Coriolis principle . . . . . 21
2.13 Schematic representation of the operating principle of an anisotropic magnetoresistive (AMR) sensing element . . . . . 22
2.14 Schematic comparison between an ideal tri-axial sensor and a non-calibrated sensor. . . . . 23
2.15 Schematic representation of an instrumented pressure insole for gait analysis . . . . . 27
2.16 Schematic representation of the operating principle of an infrared time-of-flight distance sensor . . . . . 28

3.1 Main sensing components of INDIP . . . . . 33
3.2 Right-foot wearable configuration . . . . . 33
3.3 Complete laboratory configuration of the INDIP wearable system . 34
3.4 Foot-marker configuration used for the stereophotogrammetric acquisitions . . . . . 36
3.5 Lower-limb Plug-in Gait marker set . . . . . 37

3.6 Three-dimensional reconstruction of the full-body stereophotogrammetric marker set used for the post-stroke participants. . . . . 37
3.7 Schematic representation of the standing data-personalisation procedure . . . . . 39
3.8 Schematic comparison of the straight-walking protocols adopted in the three study groups. . . . . 40
3.9 Schematic representation of the 2MWT pathway . . . . . 41
3.10 Examples of distance-sensor recordings acquired during the data-personalisation procedure . . . . . 42
3.11 Stereophotogrammetric reconstruction of the markers during the standing phase used for the alternative marker-based calibration . . 45
3.12 Overall workflow adopted for wearable stride-width estimation. . . 46
3.13 Schematic representation of the wearable stride-width estimation procedure . . . . . 48
3.14 Representative example of the wearable reconstruction used for heel-based stride-width estimation . . . . . 49
3.15 Example of three-dimensional marker reconstruction . . . . . 50
3.16 Schematic representation of the temporal matching between stereophotogrammetric (SP) and INDIP stride-width estimates. . . . . 51

4.1 Subject-level stride velocity . . . . . 56
4.2 Subject-level stereophotogrammetric reference stride width . . . . . 57
4.3 Absolute stride-width estimation error . . . . . 58
4.4 Subject-level Bland–Altman analysis . . . . . 59
4.5 Raw stride-level association . . . . . 61
4.6 Within-subject centred association . . . . . 62
4.7 Participant-reported acceptability of the wearable system among questionnaire respondents . . . . . 63
4.8 Representative foot-acceleration signals . . . . . 65
4.9 Representative inter-foot distance signals . . . . . 66

# List of Tables

3.1 Demographic and clinical characteristics of the participants . . . . . 31

4.1 Distribution of matched heel-based stride-width estimates . . . . . 54
4.2 Stride velocity and stereophotogrammetric reference stride width . . 55

# List of Abbreviations

**people with Parkinson's disease (pwPD)**

**people with post-stroke impairments (pPS)**

**healthy controls (HC)**

**Stride Width (SW)**

**Base of Support (BoS)**

**Freezing of Gait (FoG)**

**Inertial Measurement Unit (IMU)**

**magneto-inertial measurement unit (MIMU)**

**Time-of-Flight (ToF)**

**pressure insole (PI)**

**stereophotogrammetric system (SP)**

**INertial module with DIstance sensors and Pressure insoles (INDIP)**

**Two-Minute Walking Test (2MWT)**

**linear mixed-effects model (LMM)**

**confidence interval (CI)**

**minimal detectable change at the 95% confidence level ($MDC_{95}$)**

# Chapter 1

# Introduction

## 1.1 Context and motivation

Human gait is a fundamental motor function that results from the coordinated interaction of the nervous, musculoskeletal, and sensory systems. It enables forward progression while preserving postural stability and adapting to environmental changes and to the individual's physical condition. The quantitative assessment of gait can therefore provide clinically relevant information on locomotor performance, balance control, and functional mobility in both healthy individuals and people with motor impairments. Gait analysis has consequently become an important tool in clinical practice and movement research, supporting the objective characterization of walking patterns through spatiotemporal, kinematic, and kinetic parameters [1].

Among the spatial parameters used to describe gait, Stride Width (SW) provides specific information on the mediolateral regulation of foot placement and contributes, together with step length and foot orientation, to the geometrical description of the Base of Support (BoS). Since foot placement must be adjusted in response to changing locomotor demands, SW and its variability have been investigated in relation to lateral stability, balance regulation, and fall risk [2]. Its clinical relevance is particularly evident in neurological populations, such as people with Parkinson's disease (pwPD) and people with post-stroke impairments (pPS), in whom impaired motor and postural control may affect the ability to adapt foot placement.

pwPD commonly present reduced gait speed and step length, impaired rhythmicity, postural instability, and a reduced ability to modify their walking pattern according to environmental demands [3, 4]. These alterations may become more evident during complex locomotor tasks such as turning, which requires the continuous reorientation of the body and a step-by-step adjustment of foot placement. Turning may also contribute to the onset of Freezing of Gait (FoG) in susceptible individuals [5]. pPS frequently show reduced walking speed, interlimb asymmetry,

altered foot placement, and compensatory strategies associated with residual motor deficits of the paretic limb [6]. In both populations, gait impairment can reduce independence, limit participation in daily-life activities, and increase the risk of falls.

Instrumented gait assessment is traditionally performed in specialized laboratories using stereophotogrammetric systems, force platforms, or instrumented walkways. These technologies provide accurate and comprehensive measurements and are therefore commonly used as reference systems. However, they require dedicated acquisition spaces, complex instrumentation, trained operators, and time-consuming processing procedures. Moreover, laboratory assessments are generally based on short, predefined, and supervised tasks, which may not fully represent the variability of walking under everyday conditions. These constraints limit the feasibility of repeated and prolonged monitoring and may reduce the ecological validity of the assessment.

Wearable sensors provide an opportunity to extend quantitative gait analysis beyond conventional laboratories. Inertial Measurement Units (IMUs) can support the identification of gait events, the reconstruction of segment orientation and displacement, and the estimation of several spatiotemporal parameters. However, SW estimation poses a specific technological challenge: inertial data recorded from one foot can describe the motion of that foot but do not directly provide the relative position of the contralateral foot. Since SW depends on the spatial relationship between both feet, additional sensing information is required.

The INertial module with DIstance sensors and Pressure insoles (INDIP) multisensor architecture addresses this limitation by combining foot- and lower-back-mounted inertial units with pressure insoles and infrared Time-of-Flight (ToF) sensors. Foot-mounted sensors provide information on gait events and foot motion, while the lower-back unit supports the characterization of locomotor activity and changes in direction. The infrared sensors provide measurements related to the distance between the feet, enabling the reconstruction of mediolateral foot placement [7, 2]. Nevertheless, the accuracy of wearable SW estimates may depend on gait speed, walking condition, sensor geometry, processing methods, and the characteristics of the analyzed population. Validation against reference measurements across heterogeneous neurological gait patterns is therefore a necessary step toward reliable and ecologically valid SW monitoring.

## 1.2 Research gap and objectives

The inertial–infrared method underlying the present work was initially validated against stereophotogrammetry in thirteen healthy adults performing straight-walking trials at slow, comfortable, and fast self-selected speeds [2]. A subsequent

methodological development introduced a redesigned wearable configuration, revised calibration procedures, and subject-specific data personalisation, extending the assessment to both straight and curvilinear walking. However, this validation was still limited to healthy participants [8].

Therefore, the accuracy of the proposed method in neurological populations, particularly in pPS and pwPD, remains to be established. It is also necessary to determine whether its performance is affected by walking condition and by the heterogeneous gait characteristics observed in these populations, especially during turning.

The primary objective of this thesis was to validate wearable SW estimates in pPS and pwPD, using healthy controls (HC) as a comparison group and stereophotogrammetry as the reference system. Additional objectives were to quantify the estimation error, agreement, and association between wearable and reference measurements, and to assess whether measurement performance differed across populations and walking conditions. The population-by-condition interaction was specifically examined to determine whether turning affected estimation performance differently across groups. Finally, measurement uncertainty was investigated through the minimal detectable change at the 95% confidence level ($MDC_{95}$), and its clinical relevance was explored by comparison with the minimally important difference reported in the literature for SW in pwPD during straight walking.

# Chapter 2

# State of the art

## 2.1 Human gait and spatiotemporal parameters

### 2.1.1 The gait cycle

Human walking can be described as a cyclic and quasi-periodic locomotor activity, particularly during steady-state progression at a relatively constant speed. Its basic organisational unit is the gait cycle, also referred to as a stride. A gait cycle is defined as the interval between two consecutive initial contacts of the same foot with the ground. By contrast, a step extends from the initial contact of one foot to the subsequent initial contact of the contralateral foot. Therefore, one stride generally comprises two consecutive steps, one performed with each lower limb [9, 10].

Figure 2.1 illustrates the distinction between these two concepts.

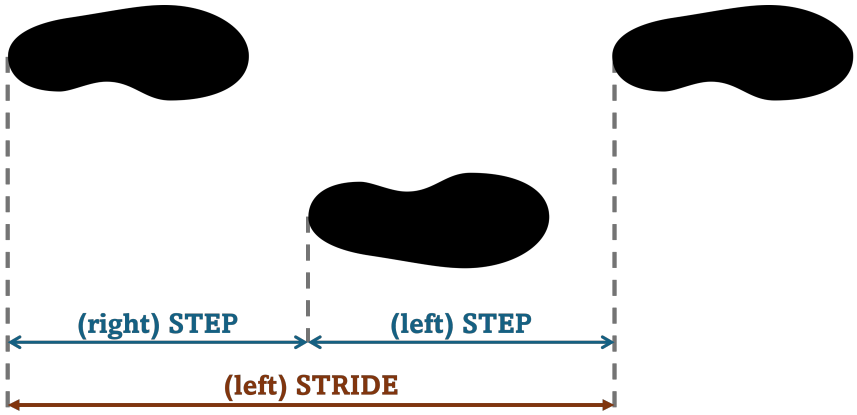



**Figure 2.1:** Schematic representation of step and stride during walking.

The left stride, for example, begins with the initial contact of the left foot, includes the subsequent right and left steps, and ends at the following initial contact of the left foot.

The gait cycle is traditionally divided into two main phases: the stance phase and the swing phase. The stance phase corresponds to the interval during which the reference foot is in contact with the ground, whereas the swing phase begins when the foot leaves the ground and continues until its subsequent initial contact. During physiological walking at a comfortable speed, stance accounts for approximately 60% of the gait cycle and swing for the remaining 40% [9, 10].

The overall temporal organisation of the gait cycle, including its functional subphases and the periods of single and double support, is illustrated in Figure 2.2.

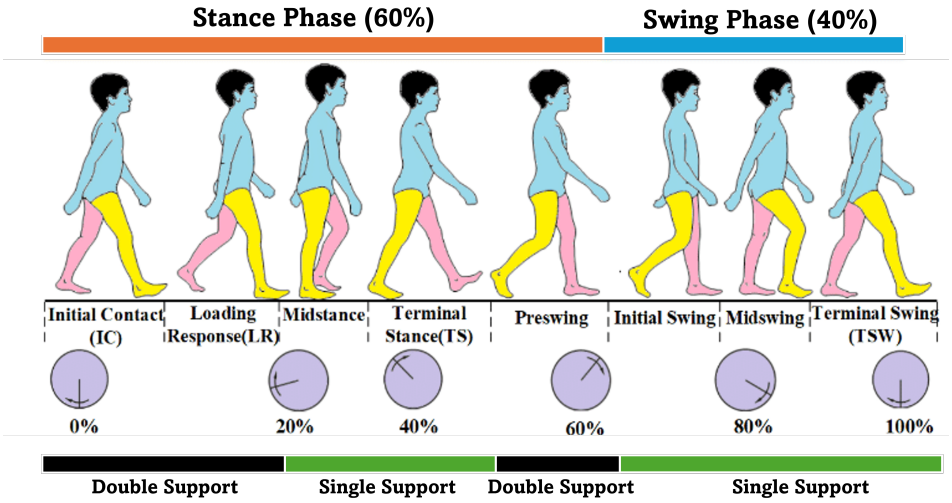



**Figure 2.2:** Main phases and functional subphases of the gait cycle. Readapted from [11].

The stance phase can be divided into five functional subphases.

It begins with *initial contact*, which occurs when the reference foot first touches the ground. In physiological gait, this event usually occurs through the heel, although different initial-contact patterns may be observed in pathological walking. The main purpose of this phase is to position the limb in preparation for weight acceptance.

Initial contact is followed by the *loading response*, during which body weight is progressively transferred onto the leading limb. Both feet are in contact with the ground during this interval. The lower limb contributes to shock absorption, weight acceptance, and maintenance of forward progression.

During *mid-stance*, the contralateral foot leaves the ground and the body progresses over the supporting limb. This subphase corresponds to a period of

single support, during which the stance limb must provide stability while allowing the body to move forward. The body centre of mass advances over the supporting foot through a mechanism commonly approximated as an inverted pendulum [12].

In *terminal stance*, the heel of the reference foot rises from the ground while the forefoot remains in contact with the supporting surface. The body continues to progress beyond the supporting foot, and the ankle plantar flexors contribute to propulsion and preparation for the subsequent transfer of body weight.

The stance phase ends with *pre-swing*, which begins with the initial contact of the contralateral foot. This subphase constitutes the second period of double support. The reference limb is progressively unloaded, the knee begins to flex, and the foot prepares to leave the ground.

The swing phase comprises three functional subphases.

During *initial swing*, the foot leaves the ground and the lower limb begins to advance. Flexion of the hip and knee and ankle dorsiflexion contribute to adequate foot clearance.

During *mid-swing*, the limb continues its forward progression and passes alongside the stance limb, while the tibia approaches a vertical position.

Finally, during *terminal swing*, the advancing limb decelerates and the knee extends, positioning the foot in preparation for the following initial contact [9, 12].

Although this phase-based organisation provides a useful reference for describing physiological walking, the timing and execution of the gait cycle can be modified by walking speed, changes in the direction of progression, and neurological or musculoskeletal impairments. The quantitative analysis of consecutive gait cycles therefore provides the basis for the definition and calculation of the main spatiotemporal gait parameters.

### 2.1.2 Main spatiotemporal gait parameters

Spatiotemporal gait parameters are objective measures of the temporal and spatial components of walking. Unlike kinematic and kinetic variables, which characterise joint motion and the forces involved in locomotion, they provide a global and readily interpretable description of gait. Consequently, they are widely used to evaluate locomotor function, detect gait abnormalities, and monitor changes over time or in response to rehabilitation interventions [9, 10].

Temporal parameters are derived from the timing of gait events. *Step time* is the interval between the initial contact of one foot and the subsequent initial contact of the contralateral foot. *Stride time*, also referred to as gait-cycle duration, is the interval between two consecutive initial contacts of the same foot. *Cadence* indicates the number of steps performed per unit of time and is generally expressed in steps per minute.

Other temporal measures quantify the duration of the main phases and support

periods of the gait cycle:

- *Stance time*: the interval during which the reference foot remains in contact with the ground;
- *Swing time*: the interval during which the reference foot advances without ground contact;
- *Single-support time*: the period during which only one foot is in contact with the ground and supports the body;
- *Double-support time*: the duration of the periods during which both feet are simultaneously in contact with the ground.

These durations may be expressed in seconds or normalised as a percentage of the gait cycle, facilitating comparisons between individuals and walking conditions [9, 10].

Spatial parameters characterise the distances and relative positions of successive foot placements. The main spatial measures considered in gait analysis are illustrated in Figure 2.3.

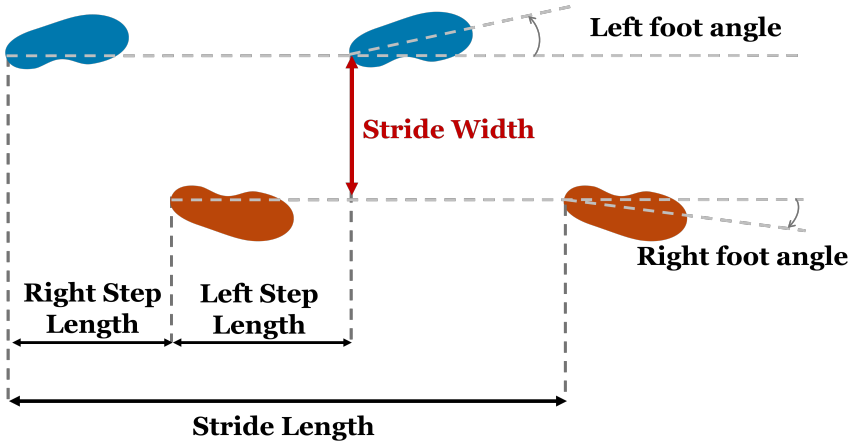



**Figure 2.3:** Schematic representation of the main spatial gait parameters, including step length, stride length, and stride width.

*Step length* is the distance measured along the direction of progression between successive initial contacts of opposite feet. *Stride length* is the distance covered between two consecutive initial contacts of the same foot and therefore spans one right and one left step [9, 10].

A further spatial parameter is *stride width*, which represents the mediolateral separation between consecutive contralateral foot placements. Whereas step length

and stride length primarily characterise forward progression, SW describes the lateral positioning of the feet during walking. Mediolateral foot placement contributes to the geometry of the BoS and to the regulation of lateral stability [2]. However, the interpretation of SW requires consideration of the locomotor context, since wider or narrower foot placement may reflect different task demands, individual strategies, or motor impairments.

The definition of spatial gait parameters requires an appropriate reference direction. During straight walking, these measures are commonly expressed relative to a fixed direction of progression. During curvilinear walking and turning, however, the direction of progression changes from one step to the next. In these conditions, step length, stride length, and mediolateral foot placement should be defined relative to a local direction that follows the participant's trajectory [13]. This consideration is particularly relevant in the present work, which includes both straight-walking and turning conditions.

*Walking speed* represents the distance travelled per unit of time and is generally expressed in metres per second. It reflects the combined contribution of spatial and temporal gait characteristics, particularly step or stride length and cadence. An increase in walking speed may result from longer steps, a higher cadence, or both, whereas slower walking is generally associated with shorter steps, a lower cadence, or a combination of these adaptations. As a concise and clinically interpretable measure of functional mobility, walking speed has been proposed as a functional vital sign [14].

In addition to their mean values, spatiotemporal parameters may be examined in terms of variability and asymmetry. *Gait variability* refers to stride-to-stride fluctuations in a given parameter and provides information that is complementary to its average value [15]. For example, SW variability quantifies the consistency of mediolateral foot placement across successive strides. Its interpretation should not be considered univocal, since both unusually low and high levels of SW variability have been associated with fall history in specific populations and walking conditions [16].

*Gait asymmetry*, by contrast, refers to differences between corresponding measures of the right and left limbs. It may be evaluated using spatial or temporal parameters, including step length, stance time, and swing time [17].

These complementary measures may identify alterations in locomotor control even when average walking speed, step length, or stride duration appear relatively preserved. Their interpretation nevertheless depends on the number of analysed strides, the walking task, and the method used for their calculation.

Spatiotemporal gait parameters may be substantially affected by neurological impairments, giving rise to characteristic and condition-specific gait patterns.

## 2.2 Gait impairments in neurological populations

Neurological disorders can affect walking by altering motor control, sensory integration, postural regulation, and the ability to adapt gait to changing locomotor demands. Although both stroke and Parkinson's disease can compromise safe and independent mobility, they affect walking through different mechanisms and give rise to distinct gait patterns. Post-stroke gait is commonly characterised by unilateral sensorimotor deficits and interlimb asymmetry, whereas gait impairment in Parkinson's disease is more closely associated with reduced movement amplitude, impaired rhythmicity, and a limited ability to adapt the walking pattern to changing locomotor demands. In both populations, impairments may become more evident when walking speed changes or when the direction of progression must be modified [6, 3].

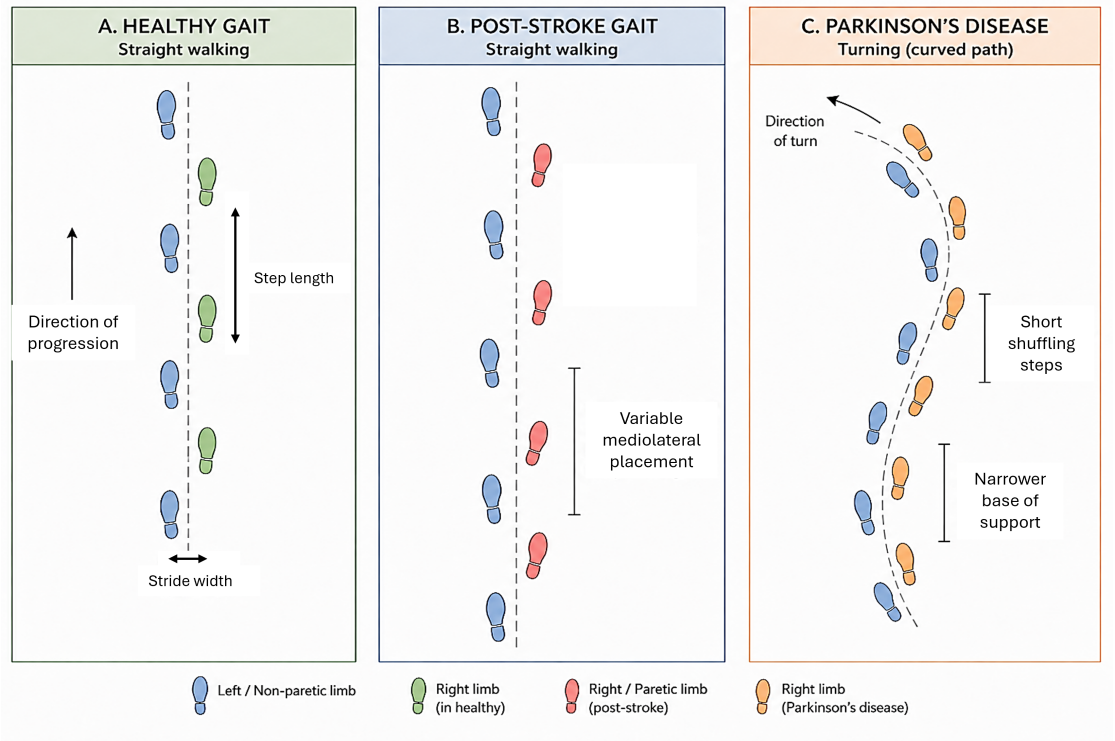



**Figure 2.4:** Schematic comparison of gait characteristics in healthy subjects, pPS, and pwPD.

### 2.2.1 Post-stroke gait impairments

The gait pattern observed after stroke is highly heterogeneous. Its characteristics depend on the location and severity of the brain lesion, the time elapsed since the

event, and the residual motor, sensory, and postural-control deficits. Weakness, spasticity, impaired selective motor control, and reduced somatosensory function may affect weight acceptance, limb advancement, propulsion, and foot clearance. Consequently, different compensatory strategies can be adopted, including pelvic elevation, circumduction of the paretic limb, and increased reliance on the non-paretic side [6].

At the spatiotemporal level, post-stroke gait is generally characterised by reduced walking speed and cadence, shorter step and stride lengths, prolonged gait-cycle and double-support durations, and spatial and temporal asymmetry. Temporal asymmetry commonly involves unequal stance and swing durations between the two limbs, with reduced support on the paretic side. Spatial asymmetry is frequently assessed through the difference between paretic and non-paretic step lengths. However, the direction of this asymmetry is not uniform across individuals: depending on the adopted compensatory strategy, either the paretic or the non-paretic step may be shorter. Therefore, separate analysis of the two limbs is more informative than assuming a single characteristic post-stroke pattern [17, 6].

Post-stroke impairments also affect the mediolateral regulation of foot placement. Although a slightly wider BoS has been reported at group level in some post-stroke populations, changes in lateral foot placement should not be interpreted as a uniform increase or reduction in SW. More specifically, the paretic limb may show a reduced ability to adjust its lateral position from one step to the next according to the motion of the body. Stimpson et al. reported a weaker relationship between pelvis dynamics and subsequent paretic step width, together with more lateral and more variable paretic foot placement. These findings suggest that post-stroke impairment may affect the active regulation of SW, rather than only its mean value [18].

Changing direction introduces additional difficulties because turning requires asymmetric modulation of the inner and outer steps, reorientation of the body, and continuous redistribution of support between the lower limbs. People with post-stroke impairments may perform turns more slowly, use a larger number of steps, and adopt different strategies depending on the side of hemiparesis and the direction of the turn. Altered coordination between body segments and preferential reliance on the non-paretic limb may further limit the ability to adapt foot placement during directional changes [19].

### 2.2.2 Gait impairments in Parkinson's disease

Gait impairment in Parkinson's disease is commonly associated with bradykinesia, rigidity, and impaired regulation of movement amplitude. A characteristic hypokinetic walking pattern may therefore emerge, with reduced walking speed, shorter steps and strides, limited lower-limb excursion, and diminished foot clearance.

The reduction in stride length is not necessarily accompanied by a proportional reduction in cadence; instead, people with Parkinson's disease may increase step frequency without adequately scaling step amplitude [20, 3].

A systematic review and meta-analysis comparing pwPD with healthy controls during self-selected straight walking identified reduced walking speed, stride length, and swing time, together with increased cadence and double-support time. These findings indicate that Parkinsonian gait affects both spatial progression and the temporal organisation of the gait cycle [4].

The effect of Parkinson's disease on mediolateral foot placement is less uniform. In pooled analyses of straight walking, mean step width did not differ significantly between pwPD and healthy controls. Therefore, a generally wider or narrower SW should not be considered an invariant feature of Parkinsonian gait. Differences may instead depend on disease severity, walking speed, medication state, and the locomotor task [4].

Directional changes place greater demands on the ability to scale movement and coordinate consecutive foot placements. Even individuals with relatively preserved straight-walking performance may display clear turning impairments. These include reduced turning speed, longer turn duration, a greater number of short steps, and reduced sequential rotation between the head, trunk, pelvis, and feet, sometimes described as an *en-bloc* turning strategy [21, 22].

The modulation of the BoS during turning may also be impaired. In contrast to healthy individuals, who generally increase the distance between the feet in response to the additional mediolateral demands of a turn, pwPD may fail to widen their foot placement sufficiently. A narrower inter-foot distance during turning has been associated with reduced margins of dynamic stability, particularly during rapid directional changes [22].

A clinically relevant manifestation of Parkinsonian gait dysfunction is FoG. It is defined as a brief and episodic absence or marked reduction of forward foot progression despite the intention to walk. Episodes may appear as progressively shorter shuffling steps, trembling of the lower limbs with little effective progression, or, less frequently, complete inability to step [23, 24].

FoG is strongly dependent on the locomotor context. It frequently occurs during gait initiation, turning, passage through doorways or narrow spaces, and dual-task walking. Among the tasks investigated in the literature, turning is one of the most effective conditions for eliciting freezing episodes [5]. In addition to limiting mobility, the sudden and unpredictable nature of FoG increases the difficulty of maintaining balance and contributes to reduced confidence during everyday walking.

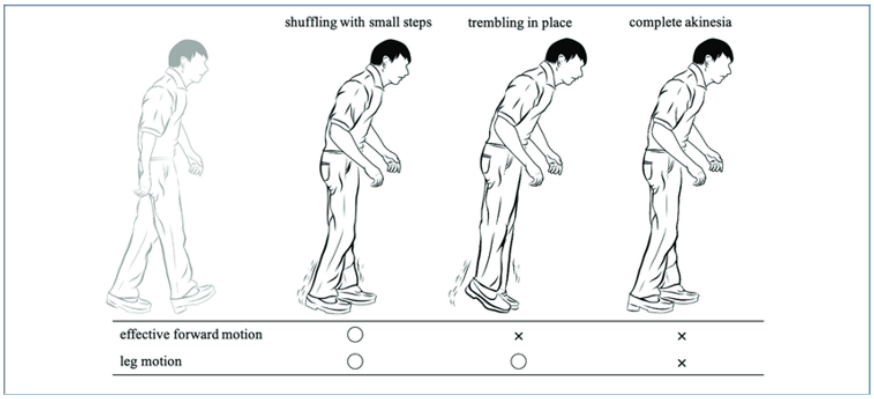



**Figure 2.5:** Schematic representation of the main manifestations of freezing of gait (FoG). Reproduced from [23].

Overall, the heterogeneous and task-dependent gait patterns observed after stroke and in Parkinson's disease highlight the need for measurement methods that remain valid across different populations and walking conditions.

## 2.3 Instrumented and wearable systems for gait analysis

Instrumented gait analysis enables the objective measurement of human movement and foot–ground interaction. Several technologies can be used to investigate specific aspects of locomotion, including spatiotemporal parameters, segment and joint kinematics, ground reaction forces, plantar pressure distribution, and muscle activation. Their suitability depends on the required level of accuracy, the measured variables, the characteristics of the investigated population, and the environment in which data are collected [25, 26].

Gait-analysis systems can be broadly distinguished into laboratory-based and wearable technologies. Laboratory systems provide detailed measurements within a controlled acquisition volume and are commonly used as reference methods. Wearable devices, by contrast, are attached directly to the participant and enable movement to be recorded across longer distances and in less constrained environments. These approaches should not be considered mutually exclusive: laboratory systems are essential for validating new measurement methods, whereas wearable technologies extend quantitative gait assessment towards more ecological conditions.

### 2.3.1 Laboratory-based systems

Stereophotogrammetry is an optical measurement technique widely used as a reference method for three-dimensional human movement analysis. Its fundamental output is the three-dimensional position of markers located within a calibrated measurement volume. In marker-based systems, multiple synchronised cameras are arranged around the acquisition space and record the two-dimensional projections of retro-reflective markers attached to the participant [27].

The reconstruction of marker position relies on stereoscopic geometry. Once the position, orientation, and optical characteristics of the cameras are known, each two-dimensional marker observation defines a line of sight extending from the camera into the measurement volume. When the same marker is simultaneously observed by multiple cameras, its three-dimensional coordinates can be obtained from the intersection, or best geometrical approximation to the intersection, of the corresponding lines of sight. This process is generally referred to as triangulation.

The resulting three-dimensional marker trajectories constitute the primary kinematic measurements provided by the stereophotogrammetric system. Segment positions and orientations, joint kinematics, foot trajectories, and spatiotemporal gait parameters are subsequently derived by combining these trajectories with an appropriate biomechanical model [27].

A typical marker-based stereophotogrammetric system consists of several synchronised optical cameras positioned so that their fields of view overlap within the measurement volume. In gait laboratories, infrared illumination is commonly used in combination with passive retro-reflective markers. The markers reflect the incident infrared radiation towards the cameras and appear as high-intensity regions in the acquired images, facilitating their detection and tracking.

The number and spatial arrangement of cameras are selected to provide sufficient coverage of the acquisition volume and to reduce the probability of marker occlusion. Since markers may become hidden by other body segments during walking, particularly during turning or when the limbs cross from a given camera perspective, observing the same region from several directions increases the robustness of three-dimensional reconstruction.

In addition to the cameras and markers, the system requires dedicated synchronisation hardware and acquisition software for image processing, marker reconstruction, labelling, and trajectory management. Calibration devices are also required to determine the geometrical relationship among the cameras and to define a common laboratory reference frame.

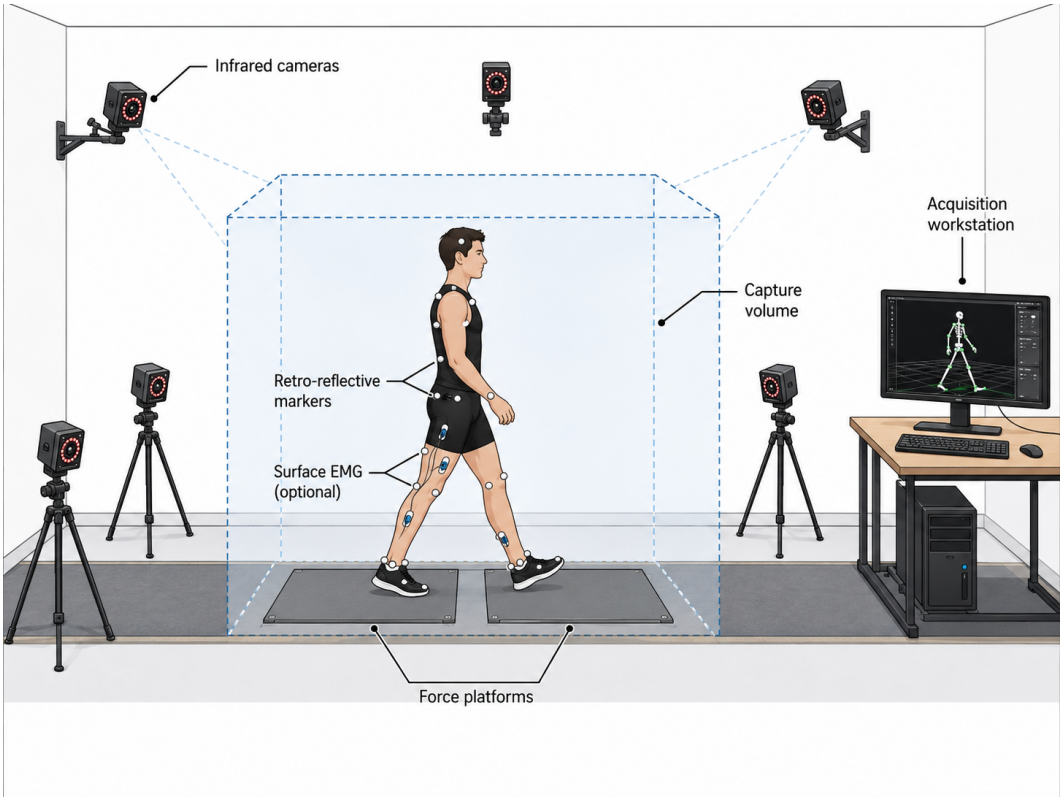



**Figure 2.6:** Typical configuration of an instrumented gait-analysis laboratory, including infrared cameras, retro-reflective markers, force platforms, an acquisition workstation, and optional surface electromyography.

Before motion acquisition, the stereophotogrammetric system must be calibrated. Camera calibration establishes the geometrical parameters required to relate two-dimensional image coordinates to positions within the three-dimensional measurement volume. These parameters include the position and orientation of each camera with respect to the laboratory reference frame, together with parameters associated with the optical system and lens distortion [28].

In commonly used motion-capture systems, calibration is performed by moving a rigid calibration object of known geometry throughout the acquisition volume. The object must be observed from different positions and orientations by the camera network, allowing the relative camera configuration to be estimated. A second calibration step defines the origin and orientation of the global laboratory coordinate system, including the horizontal plane corresponding to the laboratory floor.

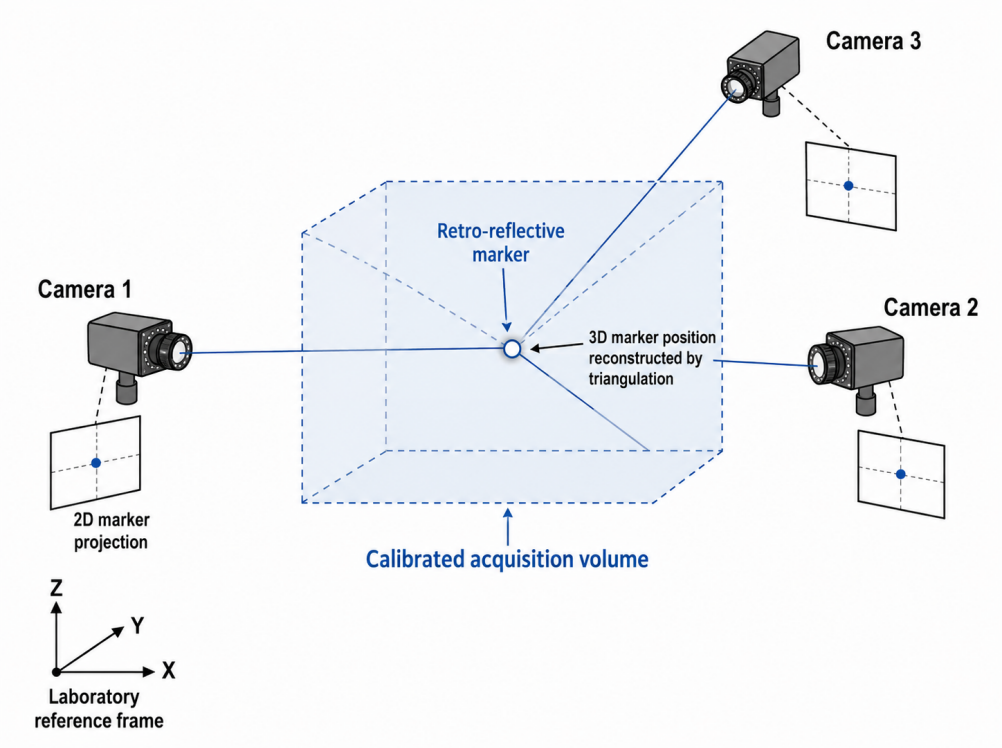



**Figure 2.7:** Principle of three-dimensional marker reconstruction in a stereophotogrammetric system

The reconstruction of marker trajectories alone does not directly provide the motion of the underlying skeletal segments. To obtain biomechanically meaningful quantities, the relationship between the measured markers and the anatomy of the participant must be established.

Markers may be positioned directly over palpable anatomical landmarks or arranged in rigid clusters attached to individual body segments. Anatomical landmarks are used to define segment-embedded anatomical reference frames and estimate joint centres and axes. Technical marker clusters, on the other hand, are primarily used to track the position and orientation of a segment during movement [27, 29].

A static or anatomical calibration acquisition is therefore commonly performed before the dynamic trials. During this acquisition, the position of selected anatomical landmarks is determined relative to the technical coordinate system of each segment. Once this relationship is known, some anatomical markers may be removed if necessary, while the segment motion can subsequently be reconstructed from the technical markers that remain attached to the participant.

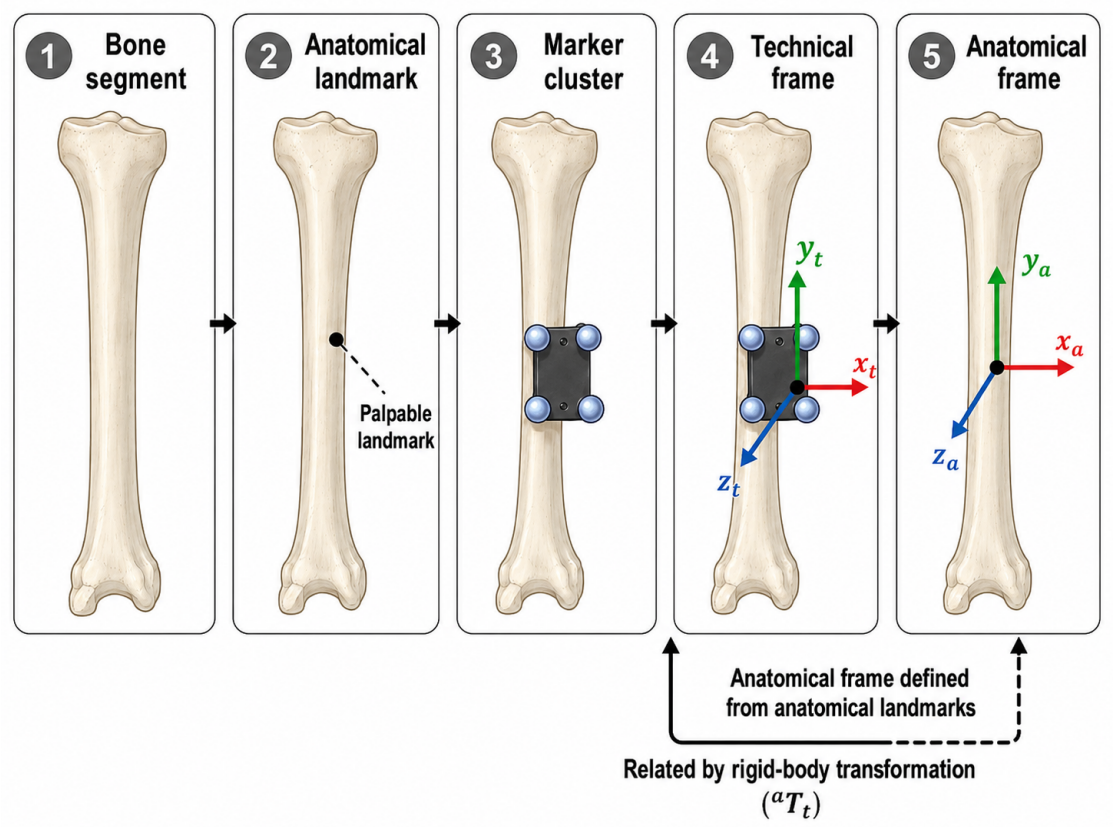



**Figure 2.8:** Schematic representation of the relationship between a bone segment, anatomical landmarks, marker clusters, and the corresponding technical and anatomical reference frames.

During dynamic acquisition, the cameras continuously record the position of the visible markers. After three-dimensional reconstruction and marker labelling, each marker is represented by a time-dependent trajectory expressed in the global laboratory reference frame. Missing portions of trajectories caused by temporary occlusions may require reconstruction or gap-filling, whereas measurement noise is generally reduced through appropriate filtering procedures [28].

For each body segment, the trajectories of the associated markers are used to estimate its instantaneous position and orientation. By expressing the orientation of one segment relative to an adjacent segment, joint rotations can subsequently be calculated according to the selected anatomical and mathematical conventions. This allows three-dimensional joint kinematics to be described in the sagittal, frontal, and transverse planes [27].

Although modern stereophotogrammetric systems can achieve very high precision in marker-position reconstruction, the accuracy variables is not determined by

the optical instrumentation alone. Errors introduced during camera calibration, marker reconstruction, anatomical landmark identification, and biomechanical modelling can propagate to the final estimates of segment and joint kinematics [28, 30]. Anatomical landmark identification represents an additional source of uncertainty. Palpable landmarks correspond to anatomical regions rather than ideal mathematical points, and their localisation may vary both within and between operators. Errors in landmark position affect the definition of segment-embedded reference frames and may propagate to joint-angle estimates, particularly to rotations of relatively small amplitude [30, 31]. A further limitation arises because markers are attached to the skin rather than directly to the underlying bones. During movement, skin and other soft tissues deform and move relative to the skeletal structures. Consequently, the measured marker trajectory contains both the motion of the underlying bone and an additional relative displacement known as soft-tissue artefact (STA). STA is one of the principal sources of uncertainty in marker-based human movement analysis and cannot be eliminated simply by increasing the optical accuracy of the camera system [32].

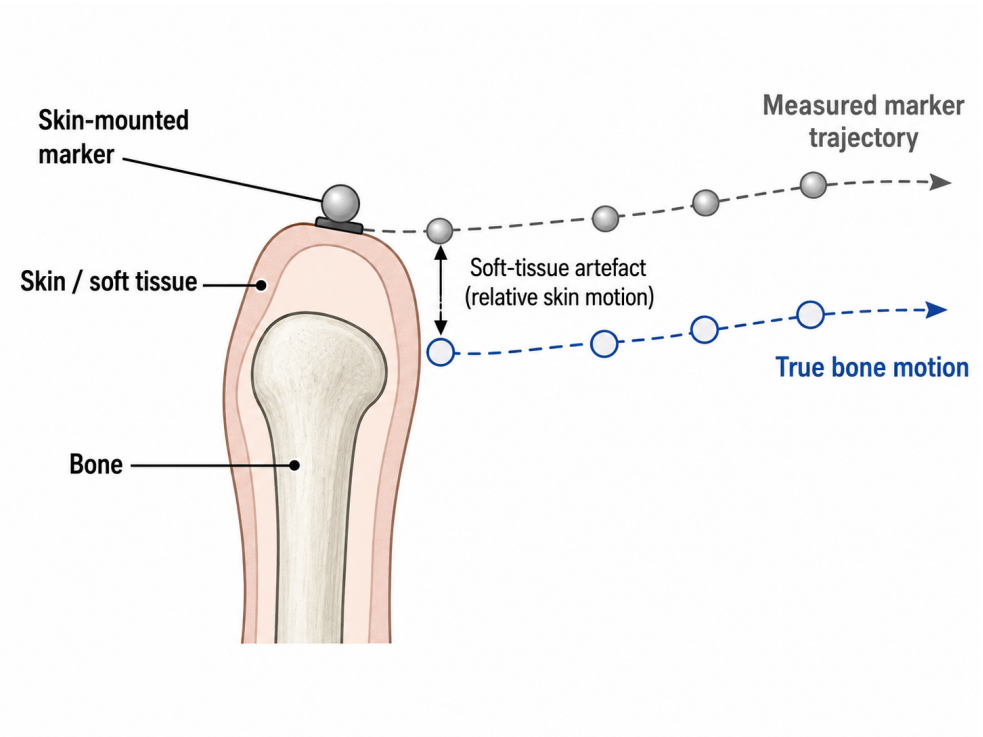



**Figure 2.9:** Schematic representation of soft-tissue artefact in marker-based motion analysis.

Despite these limitations, marker-based stereophotogrammetry remains a well-established reference technique for three-dimensional movement analysis. Its ability to provide spatially resolved marker trajectories within a common laboratory coordinate system makes it particularly suitable for the validation of novel measurement technologies.

This role is especially relevant to the present work, in which stereophotogrammetric measurements provide the reference against which wearable estimates of SW are evaluated. The specific marker configuration and processing procedure used to obtain the reference SW values are described in Chapter 3.

### 2.3.2 Wearable sensing technologies

Wearable systems reduce the dependence of gait analysis on a fixed acquisition environment by placing miniaturised sensors directly on the body or integrating them into clothing and footwear. Their portability enables longer acquisitions, repeated assessments, and the investigation of walking under structured, semi-structured, or real-world conditions. However, unlike optical motion-capture systems, wearable sensors do not directly provide the position of anatomical landmarks within a global reference frame. Biomechanically meaningful quantities must therefore be derived from the recorded signals through calibration, signal-processing, sensor-fusion, and biomechanical modelling procedures [25, 26].

#### Magneto-inertial sensing

Among wearable technologies, magneto-inertial measurement units (MIMUs) are extensively used for human movement and gait analysis. A MIMU typically combines a tri-axial accelerometer, a tri-axial gyroscope, and a tri-axial magnetometer. These sensing modalities provide complementary information: the accelerometer measures specific force, the gyroscope measures angular velocity, and the magnetometer measures the local magnetic-field vector. Their signals can subsequently be combined to estimate sensor orientation and describe its motion with respect to an external reference frame [33, 34]. The accelerometer is the inertial sensing element responsible for measuring specific force along three mutually orthogonal axes. Modern wearable inertial units generally employ micro-electromechanical systems (MEMS), in which the sensing structure is manufactured at a microscopic scale.

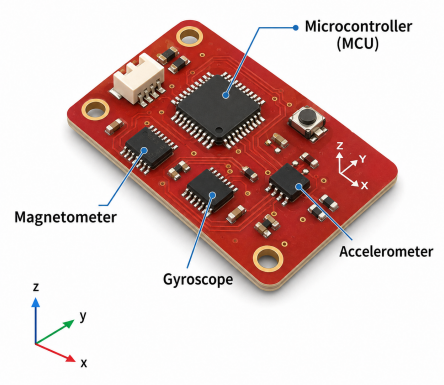



**Figure 2.10:** Typical architecture of a wearable magneto-inertial measurement unit (MIMU).

In a capacitive MEMS accelerometer, the sensing element can be represented as a proof mass suspended by elastic structures. When the sensor housing is accelerated, the inertia of the proof mass produces a relative displacement with respect to the surrounding structure. This displacement modifies the distance between movable and fixed electrodes and therefore changes their capacitance. A differential configuration is commonly adopted so that displacement of the proof mass causes opposite variations in two capacitances, which are converted by the electronic interface into an acceleration-related signal.

A simplified one-dimensional mechanical model of the sensing element can be described as a mass–spring–damper system:

$$m\ddot{x} + c\dot{x} + kx = -ma_x, \tag{2.1}$$

where $m$ is the proof mass, $c$ is the damping coefficient, $k$ is the equivalent elastic stiffness, $x$ is the displacement of the proof mass relative to the sensor housing, and $a_x$ is the acceleration of the housing along the sensing axis.

An accelerometer does not directly measure translational acceleration, but the *specific force* acting along its sensing axes. In an ideal sensor, specific force can be expressed as

$$\mathbf{f} = \mathbf{a} - \mathbf{g}, \tag{2.2}$$

where $\mathbf{f}$ is the measured specific force, $\mathbf{a}$ is the translational acceleration of the sensor, and $\mathbf{g}$ is the gravitational acceleration vector. Consequently, the accelerometer output depends both on sensor motion and on its orientation relative to gravity.

If the orientation of the sensor frame $S$ with respect to a global frame $G$ is known, the translational acceleration can be reconstructed as

$$\mathbf{a}^G = \mathbf{R}_S^G \mathbf{f}^S + \mathbf{g}^G, \tag{2.3}$$

where $\mathbf{R}_S^G$ is the rotation matrix that transforms a vector expressed in the sensor frame into the global reference frame. Accurate orientation estimation is therefore essential when accelerometric measurements are used to reconstruct translational motion. Under static or quasi-static conditions, the accelerometer signal is dominated by the gravity-related component and can therefore provide information about sensor inclination. During dynamic motion, however, motion-related components are superimposed on this contribution, making the gravity direction less directly observable.

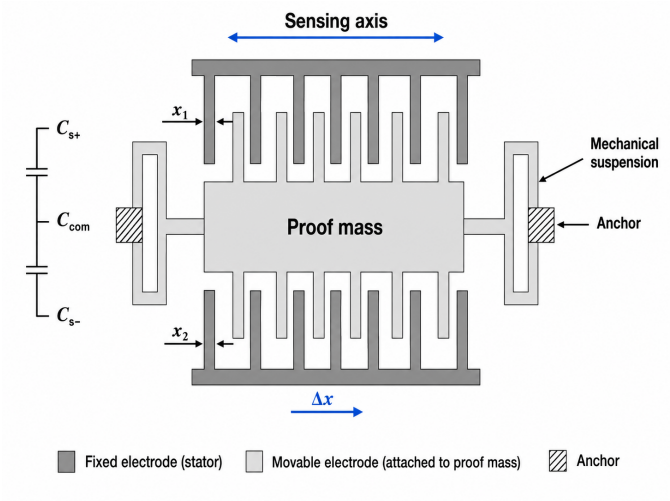



**Figure 2.11:** Schematic representation of one sensing axis of a capacitive MEMS accelerometer. The proof mass is suspended by a mechanical structure and connected to movable comb electrodes. A displacement $\Delta x$ along the sensing axis changes the gaps between fixed and movable electrodes, producing opposite variations in the differential capacitances.

Gyroscopes complement accelerometers by measuring rotational motion. A tri-axial gyroscope provides the angular-velocity vector of the sensor about three mutually orthogonal sensing axes. MEMS gyroscopes are commonly based on vibrating microstructures that exploit the Coriolis effect. A proof mass is maintained in oscillation along a drive direction; when the sensor undergoes rotation, the interaction between the imposed vibration and the angular motion generates a Coriolis force that produces a secondary displacement along an orthogonal sense direction.

The Coriolis force acting on the vibrating proof mass can be expressed as

$$\mathbf{F}_C = 2m\,(\mathbf{v}_d \times \boldsymbol{\omega})\,, \tag{2.4}$$

where $m$ is the vibrating proof mass, $\mathbf{v}_d$ is its velocity along the drive axis, and $\boldsymbol{\omega}$ is the angular velocity of the sensor.

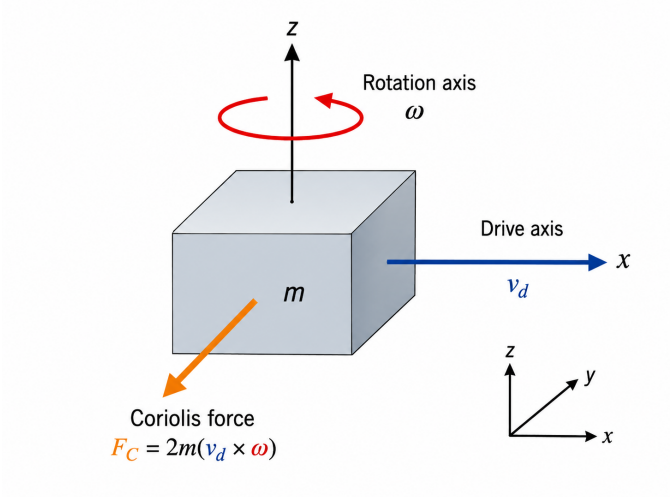



**Figure 2.12:** Schematic representation of the Coriolis principle underlying a vibrating MEMS gyroscope. A proof mass $m$ oscillates along the drive axis with velocity $\mathbf{v}_d$; when the sensor rotates with angular velocity $\boldsymbol{\omega}$, a Coriolis force $\mathbf{F}_C = 2m(\mathbf{v}_d \times \boldsymbol{\omega})$ arises along an orthogonal direction.

The angular velocity measured by a gyroscope can be represented by the simplified model

$$\boldsymbol{\omega}_m(t) = \boldsymbol{\omega}(t) + \mathbf{b}_\omega(t) + \mathbf{n}_\omega(t), \tag{2.5}$$

where $\boldsymbol{\omega}$ is the actual angular velocity, $\mathbf{b}_\omega$ represents the gyroscope bias, and $\mathbf{n}_\omega$ represents measurement noise.

Angular velocity can be integrated over time to estimate changes in sensor orientation. However, even when the sensor is stationary, the gyroscope output may exhibit a non-zero offset, commonly referred to as *zero-rate bias*. A constant component of this bias can in principle be estimated and compensated, whereas residual bias variations and stochastic effects remain. Since these errors are integrated together with the true angular velocity, they progressively accumulate and give rise to orientation drift [35, 34].

The third sensing modality integrated into a MIMU is the magnetometer, which measures the local magnetic-field vector along three orthogonal axes. Different technologies can be employed for magnetic sensing. Among these, anisotropic

magnetoresistive (AMR) sensors exploit the dependence of the electrical resistance of a ferromagnetic material on the relative orientation between its magnetisation and the direction of the electric current [36].

For orientation estimation, the magnetometer provides an external directional reference through measurement of the local Earth's magnetic field. This information complements the gravity-related reference obtained from the accelerometer and can contribute to limiting the accumulation of heading error associated with gyroscope integration [33].

Magnetic measurements are, however, particularly sensitive to the surrounding environment. Ferromagnetic materials, electrical equipment, and electric currents can alter the local magnetic field and therefore affect orientation estimation. Magnetic distortions are commonly classified into *hard-iron* effects, which introduce an approximately constant offset in the measured field, and *soft-iron* effects, which alter its magnitude and direction. Appropriate calibration and, when necessary, compensation strategies are therefore required before magnetometer data are used as an orientation reference [33].

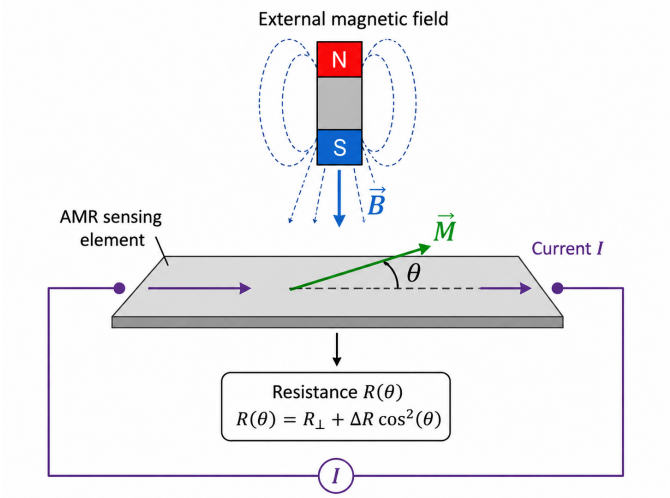



**Figure 2.13:** Schematic representation of the operating principle of an anisotropic magnetoresistive (AMR) sensing element. The electrical resistance of the ferromagnetic material depends on the angle $\theta$ between the magnetisation vector $\mathbf{M}$ and the direction of the electric current $I$. An external magnetic field modifies the magnetisation direction and, consequently, the measured resistance according to $R(\theta) = R_\perp + \Delta R \cos^2 \theta$.

Before inertial and magnetic signals can be used for quantitative movement analysis, sensor-specific measurement errors must be considered. MEMS sensors may be affected by bias, scale-factor errors, cross-axis sensitivity, non-orthogonality of

the sensing axes, temperature-dependent effects, and stochastic noise. A simplified measurement model can be written as

$$\mathbf{y} = \mathbf{K}\mathbf{x} + \mathbf{b} + \mathbf{n}, \tag{2.6}$$

where $\mathbf{x}$ represents the physical quantity to be measured, $\mathbf{y}$ is the sensor output, $\mathbf{K}$ contains scale-factor and axis-misalignment terms, $\mathbf{b}$ represents sensor bias, and $\mathbf{n}$ represents random noise. Calibration procedures aim to estimate the systematic components of this model and compensate for them before subsequent processing [37, 38].

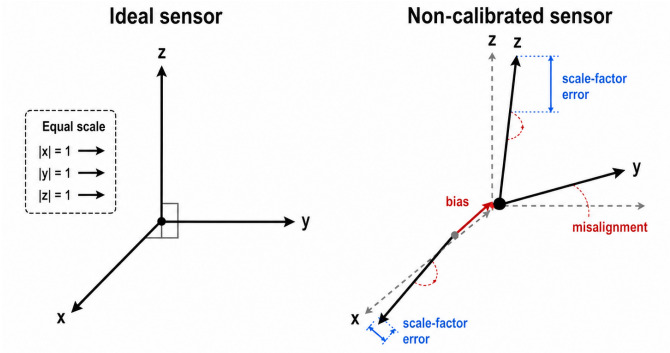



**Figure 2.14:** Schematic comparison between an ideal tri-axial sensor and a non-calibrated sensor.

Accurate three-dimensional orientation cannot generally be obtained from any of the three sensing modalities considered independently. The gyroscope provides reliable information on short-term rotational changes but is affected by integration drift. The accelerometer provides a gravity-related reference under sufficiently low dynamic conditions but is also sensitive to translational accelerations. The magnetometer provides an additional directional reference but can be affected by environmental magnetic disturbances.The three measurements are therefore complementary. In particular, the gravity-related direction obtained from the accelerometer provides information about sensor inclination but does not independently determine rotation about the gravity direction. The magnetic-field vector supplies an additional directional reference that can contribute to heading estimation. Sensor-fusion algorithms combine these measurements to exploit their complementary characteristics and obtain a more stable estimate of sensor orientation. Different approaches have been proposed, including complementary filters and Kalman-filter-based methods, as well as computationally efficient orientation filters specifically developed for wearable inertial sensing [33, 34].

Three-dimensional orientation is commonly represented using rotation matrices or unit quaternions. Quaternions are particularly convenient because they provide

a compact representation of three-dimensional rotation without the singularities associated with some angle-based parameterisations. Let $\mathbf{q}_S^G$ denote the unit quaternion describing the orientation of the sensor frame $S$ with respect to the global frame $G$:

$$\mathbf{q}_S^G = \begin{bmatrix} q_0 & q_1 & q_2 & q_3 \end{bmatrix}^T, \qquad \left\| \mathbf{q}_S^G \right\| = 1. \tag{2.7}$$

Using the convention in which $\mathbf{q}_S^G$ rotates vectors from the sensor frame to the global frame and angular velocity is expressed in the sensor frame, quaternion kinematics can be written as

$$\dot{\mathbf{q}}_S^G = \frac{1}{2} \mathbf{q}_S^G \otimes \begin{bmatrix} 0 \\ \boldsymbol{\omega}^S \end{bmatrix}, \tag{2.8}$$

where $\otimes$ denotes quaternion multiplication. Gyroscope integration provides the short-term evolution of orientation, while accelerometer and magnetometer measurements can be incorporated by the sensor-fusion algorithm to constrain the estimate and reduce long-term drift [34].

Orientation errors are particularly relevant when inertial sensing is used to reconstruct translational motion. An inaccurate orientation estimate results in an incorrect transformation of the accelerometer measurements and an incorrect compensation of the gravitational contribution. Even a small residual acceleration error is subsequently integrated once to estimate velocity and a second time to estimate position. Consequently, errors can accumulate rapidly along the processing chain from orientation to acceleration, velocity, and displacement.

In gait analysis, MIMUs can be positioned on different body segments depending on the variables of interest. Sensors mounted on the lower limbs can support gait-event detection and the estimation of temporal parameters, whereas foot-mounted units are particularly suitable for reconstructing foot orientation, velocity, and displacement. Sensors positioned on the trunk or lower back can instead provide information on whole-body locomotor activity and changes in the direction of progression [26, 39].

Foot-mounted inertial sensing is particularly relevant for the estimation of spatial gait parameters. After orientation has been estimated, the measured specific force can be transformed into a global reference frame and compensated for gravity. The resulting translational acceleration can then, in principle, be integrated to obtain sensor velocity:

$$\mathbf{v}^G(t) = \mathbf{v}^G(t_0) + \int_{t_0}^{t} \mathbf{a}^G(\tau)\, d\tau, \tag{2.9}$$

and subsequently position:

$$\mathbf{p}^G(t) = \mathbf{p}^G(t_0) + \int_{t_0}^{t} \mathbf{v}^G(\tau)\, d\tau. \tag{2.10}$$

Direct integration is highly sensitive to residual sensor bias, noise, and orientation errors, which cause velocity and position estimates to drift. Foot-mounted sensors offer an important advantage in this respect because short intervals during which the foot can be approximated as stationary may occur during stance, typically around the flat-foot period. Once these intervals have been identified, the approximately zero-velocity condition can be used to constrain the reconstructed velocity and reduce the accumulation of integration error [40, 41].

This approach has enabled foot-mounted inertial systems to estimate several spatial gait quantities, including stride length, stride velocity, foot clearance, and changes in walking direction [40, 41]. Nevertheless, the performance of the resulting estimates depends not only on the intrinsic characteristics of the sensors but also on calibration quality, sensor placement, sensor-to-segment alignment, orientation estimation, gait-event detection, drift-correction strategies, and the assumptions incorporated into the processing algorithms. Since inertial measurements are expressed in a sensor-fixed reference frame, appropriate alignment or calibration procedures are required to relate the measured quantities to biomechanically meaningful directions. Nevertheless, once these methodological aspects are properly addressed, MIMU-based gait analysis offers several practical advantages, including sensor miniaturisation, portability, relatively low cost, and the possibility of collecting repeated or prolonged measurements beyond the laboratory. These characteristics make wearable inertial sensing particularly suitable for extending gait analysis towards less constrained and more ecologically representative conditions.

At the same time, pathological gait can pose additional challenges to MIMU-based processing methods. Altered lower-limb kinematics, irregular gait events, changes in stance behaviour, and atypical movement patterns may reduce the validity of assumptions derived from healthy straight walking. The sensor configuration and processing algorithms must therefore be validated in the specific populations and locomotor conditions for which they are intended [39].

### Pressure insoles

Instrumented pressure insoles provide information about the interaction between the plantar surface of the foot and the ground while preserving the portability of a wearable measurement system. Unlike inertial sensors, which infer gait events from characteristic patterns in acceleration or angular velocity, pressure-sensing elements provide a direct indication of foot–ground loading and unloading. This makes pressure insoles particularly useful for identifying temporal events of the gait cycle and for characterising plantar loading during walking [42].

Instrumented insoles can incorporate different sensing technologies, including resistive, piezoresistive, capacitive, and piezoelectric elements. A commonly adopted solution in wearable gait-analysis systems is based on force-sensing resistors (FSRs). These sensors consist of pressure-sensitive resistive materials whose electrical resistance changes when a normal load is applied. As the applied force increases, the resistance generally decreases, allowing changes in plantar loading to be converted into an electrical signal. Multiple sensing elements can be distributed over the plantar surface to provide spatial information about the regions of the foot that are loaded during the different phases of the gait cycle.

For gait analysis, the temporal evolution of plantar-pressure signals can be used to identify events such as initial contact and final contact and, consequently, to determine stance and swing intervals. When several sensing elements are distributed across different plantar regions, the progression of loading from the heel towards the forefoot can also provide a more detailed description of foot–ground interaction. In particular, combining information from multiple pressure-sensitive regions can improve the robustness of gait-event detection compared with the use of a single pressure threshold [42].

Pressure insoles offer several advantages for wearable gait assessment. Since they are placed inside the footwear, they allow consecutive steps to be recorded without restricting walking to an instrumented area of the floor. They can therefore support prolonged acquisitions and measurements outside conventional gait laboratories. Moreover, the direct measurement of foot–ground interaction provides information that is complementary to the motion-related signals recorded by inertial sensors.

Their performance nevertheless depends on several factors. Pressure-sensing elements may exhibit non-linearity, hysteresis, drift, and variability between sensors, while the measured load distribution can be affected by sensor placement, footwear characteristics, foot morphology, and changes in the position of the insole inside the shoe. The number and spatial distribution of sensing elements also influence the amount of plantar information that can be reconstructed. Consequently, appropriate calibration and signal-processing procedures are required according to the intended application.

For wearable gait analysis, however, a complete reconstruction of plantar pressure is not always necessary. Low-spatial-resolution insoles can instead be used primarily to obtain reliable information on foot contact. Salis et al. demonstrated that gait events can be identified from insoles equipped with a limited number of pressure-sensing elements by exploiting the redundancy and spatial distribution of the recorded signals [42]. This approach is particularly relevant to multi-sensor architectures, in which pressure information can complement inertial measurements for gait-cycle segmentation.

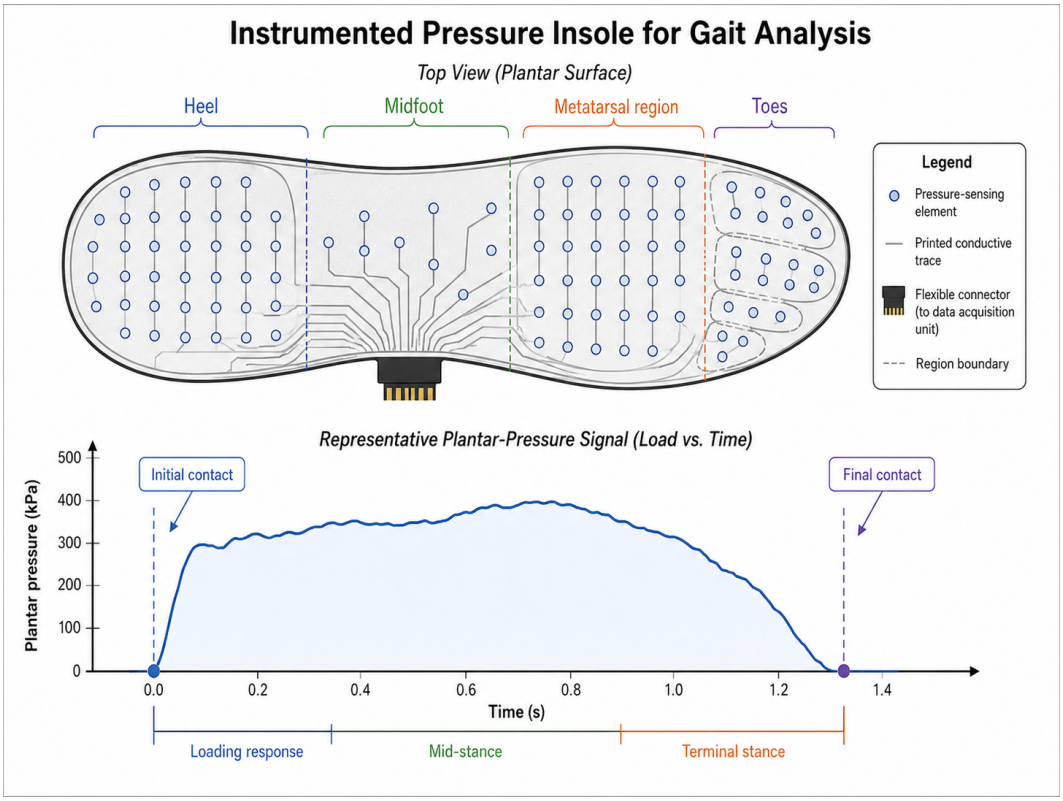



**Figure 2.15:** Schematic representation of an instrumented pressure insole for gait analysis. Pressure-sensing elements are distributed across the heel, midfoot, metatarsal region, and toes. A representative plantar-pressure signal is shown below, highlighting the identification of initial contact and final contact during stance.

### Infrared time-of-flight distance sensors

Although foot-mounted inertial sensors can reconstruct the motion of an instrumented foot, they do not directly measure its instantaneous position relative to the contralateral foot. This represents an important limitation when gait parameters depend explicitly on the spatial relationship between the two feet. Wearable distance sensors provide a complementary measurement by directly assessing the separation between the sensor and a target located on, or represented by, the opposite foot [43, 2].

Among the available ranging technologies, infrared time-of-flight (ToF) sensors provide a compact solution for short-range distance measurements. A ToF sensor emits infrared radiation towards a target and detects the reflected signal. Distance is estimated from the propagation time required by the emitted light to reach the target and return to the receiver. In its simplest representation, the relationship

can be written as

$$d = \frac{c\,\Delta t}{2}, \tag{2.11}$$

where $d$ is the sensor-to-target distance, $c$ is the speed of light, and $\Delta t$ is the measured round-trip propagation time. The factor $1/2$ accounts for the outward and return paths of the emitted radiation.

Compared with ranging methods based primarily on the intensity of the reflected signal, ToF sensing estimates an absolute distance from propagation information and can therefore reduce sensitivity to variations in target reflectance. Nevertheless, measurement performance remains dependent on the geometry of the sensor–target interaction, including the distance, relative orientation, incidence angle, field of view, and visibility of the target [43].

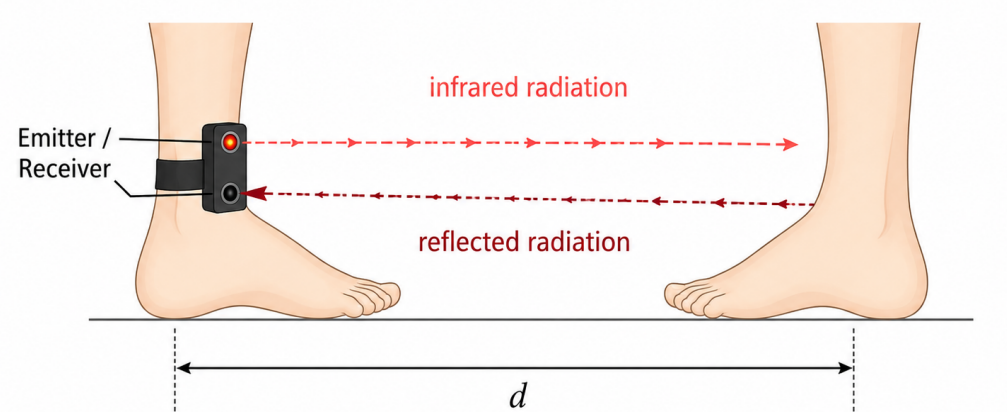



**Figure 2.16:** Schematic representation of the operating principle of an infrared time-of-flight distance sensor. The sensor emits infrared radiation towards the contralateral foot and detects the reflected signal.

The use of infrared ToF sensors for human-movement analysis has been investigated specifically for short-range measurements between body segments. Bertuletti et al. evaluated the static and dynamic performance of a miniaturised wearable platform integrating a magneto-inertial unit and an infrared ToF sensor under conditions representative of lower-limb motion. Their results showed that measurement error was strongly influenced by the angle of incidence between the sensor and the target, particularly during dynamic motion [43]. This aspect is especially relevant during gait, since the relative position and orientation of the feet continuously change throughout the gait cycle.

Direct inter-foot distance measurements have subsequently been used to complement inertial sensing during walking. A wearable configuration combining one inertial unit with two infrared ToF sensors positioned on the medial side of

one foot was proposed to detect steps through changes in the measured distance between the feet. This approach demonstrated that direct ranging can provide information on both ipsilateral and contralateral steps without relying exclusively on impact-related inertial features [44].

Distance measurements are particularly relevant to the estimation of spatial parameters associated with the relative placement of the feet. However, the raw distance measured by a ToF sensor should not be interpreted directly as SW. The sensor provides a range measurement along its instantaneous line of sight, whereas SW is defined according to the geometry of the two feet and the direction of progression. Estimating SW therefore requires the distance measurements to be combined with information about foot position and orientation and with an appropriate geometrical model [2].

This complementary use of inertial and distance information addresses a fundamental limitation of foot-mounted inertial sensing. The inertial units provide the temporal evolution of foot motion and orientation, whereas the infrared sensors introduce a direct observation of the relative geometry between the feet. Their integration enables spatial quantities related to inter-foot placement to be estimated without requiring an external laboratory-based positioning system [2].

### Multi-sensor integration

The complementary characteristics of inertial units, pressure insoles, and distance sensors motivate their integration within multi-sensor wearable architectures. Each sensing modality provides information that is difficult to obtain robustly from the others: inertial units describe segment motion and orientation, pressure insoles directly characterise foot–ground contact, and distance sensors provide measurements related to the relative position of the feet.

Combining these signals can therefore reduce the dependence of gait estimation on a single sensing principle and provide a more complete description of locomotion. In particular, pressure measurements can support gait-event identification, inertial measurements can be used to reconstruct foot trajectories, and inter-foot distance measurements can supplement these trajectories with information on the relative geometry of the two feet.

This multi-sensor principle underlies the INDIP architecture, which integrates inertial units, plantar pressure insoles, and distance sensors in a wearable system designed for gait assessment under both controlled and real-world conditions [7]. The combination of these technologies is particularly relevant when the variables of interest depend not only on the motion of individual body segments but also on their relative spatial configuration.

# Chapter 3

# Materials and methods

## 3.1 Participants and clinical characterization

The present study included a total of 30 participants belonging to three populations: 18 healthy controlss (HCs), six pPSs, and six pwPDs. The participants originated from three different experimental cohorts and were therefore recruited and assessed according to the corresponding parent-study protocols. Consequently, the available demographic and clinical descriptors were not completely homogeneous across groups.

The HC group consisted of the same 18 participants previously recruited for the development and validation of the wearable method for the estimation of base-of-support parameters [8]. Participants were recruited and assessed at the PoliTOBIOMed Laboratory of Politecnico di Torino. The group included nine females and nine males, with a mean age of $28.6 \pm 9.0$ years (range: 20–62 years), a mean height of $171.9 \pm 7.6$ cm, and a mean body mass of $67.3 \pm 10.8$ kg. Eligibility required the absence of neurological or musculoskeletal impairments potentially affecting gait and the ability to complete the experimental protocol. None of the participants used a walking aid during the experimental assessment.

The pwPD group consisted of six participants recruited within the MOVEWISE (Mobility Observation Via Wearable Integrated Sensor Evaluation) study at the IRCCS Istituto Auxologico Italiano, Division of Neurology and Neurorehabilitation, Piancavallo. All participants considered in the present analysis were assessed at the first study time point (T1). According to the MOVEWISE eligibility criteria, participants with Parkinson's disease were required to be at least 18 years old, have a diagnosis of Parkinson's disease according to the Movement Disorder Society diagnostic criteria, and have a Mini-Mental State Examination score of at least 24/30. General eligibility criteria additionally required the ability to walk independently for at least 4 m, with or without a walking aid, the ability to

provide informed consent, and willingness to wear the experimental setup. Main exclusion criteria included recent major cardiovascular or cerebrovascular events and medical conditions that could interfere with study participation; mobility limitations attributable to conditions other than Parkinson's disease also represented a disease-specific exclusion criterion.

The six pwPDs included in the present analysis had a mean age of $67.8 \pm 8.9$ years (range: 58–81 years), a mean height of $169.3 \pm 8.2$ cm, and a mean body mass of $72.0 \pm 16.9$ kg. Disease severity ranged from stage 2 to stage 4 on the Hoehn and Yahr scale, thereby including participants with mild to more advanced motor impairment. Walking-aid use was heterogeneous within the group, with documented use ranging from no aid to a unilateral crutch or a four-wheel walker.

The pPS group consisted of six participants recruited within the GaitCAP (From Capacity to Performance) study conducted at the Lake Lucerne Institute. All participants included in the present analysis were assessed at T1. According to the GaitCAP eligibility criteria, participants were required to be at least 18 years old and able to walk independently, with or without a walking aid, for a minimum of 200 m and for at least 10 m without interruption. Participants were also required to understand the study instructions, be willing to wear the experimental sensor setup, and provide written informed consent.

The six pPSs had a mean age of $68.2 \pm 13.5$ years (range: 42–79 years), a mean height of $175.2 \pm 12.1$ cm, and a mean body mass of $73.8 \pm 13.8$ kg. Five participants did not use a walking aid during the experimental assessment, whereas one participant used a unilateral walking stick. Additional stroke-specific clinical descriptors, such as time since stroke, paretic side, or clinical severity scores, were not available in the dataset used for the present analysis.

Table 3.1 summarises the demographic and clinical characteristics available for the three populations. Since the participants originated from different parent studies, some variables were not available for all cohorts.

**Table 3.1:** Demographic and clinical characteristics of the participants included in the present study. Continuous variables are reported as mean ± standard deviation. N/A indicates information not available in the dataset used for the present analysis.

| **Characteristic** | **HC** | **pPS** | **pwPD** |
|---|---|---|---|
| Participants, $n$ | 18 | 6 | 6 |
| Age, years | $28.6 \pm 9.0$ | $68.2 \pm 13.5$ | $67.8 \pm 8.9$ |
| Age range, years | 20–62 | 42–79 | 58–81 |
| Height, cm | $171.9 \pm 7.6$ | $175.2 \pm 12.1$ | $169.3 \pm 8.2$ |
| Body mass, kg | $67.3 \pm 10.8$ | $73.8 \pm 13.8$ | $72.0 \pm 16.9$ |
| Sex, F/M | 9/9 | N/A | N/A |
| Walking-aid users | 0/18 | 1/6 | 2/6 |

## 3.2 Experimental instrumentation

Gait data were acquired using two complementary measurement systems: the INDIP wearable system and a stereophotogrammetric motion-capture system. The wearable system provided inertial, plantar-pressure, and inter-foot distance measurements, whereas stereophotogrammetry was used as the laboratory reference for the three-dimensional reconstruction of foot motion. Although the three participant groups originated from different parent studies and acquisition centres, the foot-mounted wearable configuration relevant to stride-width estimation was kept consistent across datasets. In particular, the right foot was always equipped with the rigid support developed in the previous methodological work [8], hosting one MIMU and two infrared ToF distance sensors.

### 3.2.1 INDIP wearable system

The INDIP (INertial module with DIstance sensors and Pressure insoles) system is a modular wearable platform developed for the assessment of human mobility in laboratory and out-of-laboratory conditions [7, 2]. The system combines magneto-inertial sensing with plantar-pressure measurements and short-range infrared distance sensing, allowing complementary information on segment motion, foot–ground contact, and relative foot position to be collected within the same wearable architecture.

The complete laboratory configuration included multiple MIMUs, two instrumented pressure insoles, and two infrared distance sensors. The magneto-inertial units integrated a tri-axial accelerometer and gyroscope (LSM6DSO, STMicroelectronics) together with a tri-axial magnetometer (LIS2MDL, STMicroelectronics). The accelerometer operated over a measurement range of $\pm 16$ g, the gyroscope over $\pm 2000$ deg/s, and the magnetometer over $\pm 50$ Gauss. Magneto-inertial signals were sampled at 100 Hz [2, 8].

The main sensing components of the INDIP system are shown in Figure 3.1.

In the configuration adopted for the laboratory acquisitions, one MIMU was mounted on each foot. Additional units could be placed on the lower back, approximately at the level of the L5 vertebra, and on the head according to the specific parent-study protocol. A dedicated additional unit could also be used as a trigger for synchronisation with the stereophotogrammetric system. Since the present work focuses on stride-width estimation, the two foot-mounted units and the associated distance-sensing system represented the components of primary interest.

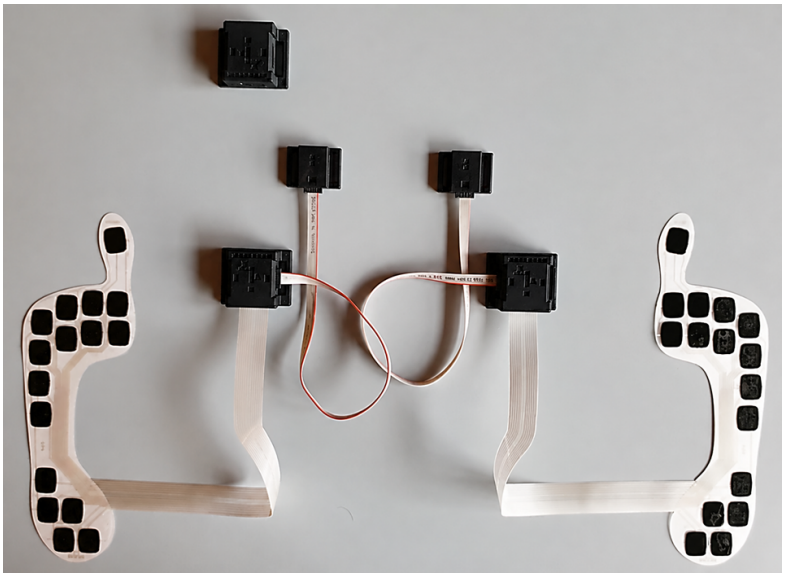


**Figure 3.1:** Main sensing components of the INDIP wearable system, including the inertial modules, the infrared distance sensors, and the two instrumented pressure insoles.

The left-foot MIMU was fixed to the shoe laces using a dedicated clip. The right-foot configuration was more complex and reproduced the refined setup previously introduced by [8]. A rigid three-dimensional printed support was attached to the medial side of the right shoe by means of a Velcro strap. The support had an approximately L-shaped geometry and accommodated the right-foot MIMU in its posterior portion and two infrared distance sensors along its medial arm. The support ensured a fixed geometrical relationship among the three sensing elements throughout the acquisition.

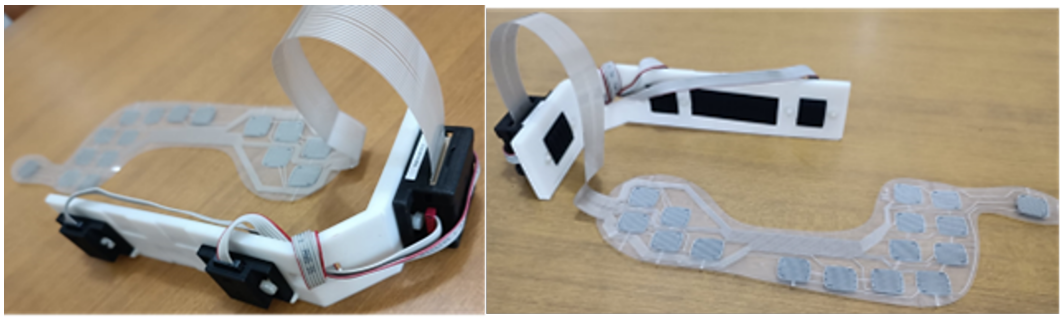


**Figure 3.2:** Right-foot wearable configuration adopted in the present study, shown from two different viewpoints.

The two distance sensors were oriented towards the medial surface of the contralateral foot. This arrangement was specifically designed to provide direct information on the relative position of the feet during walking, which cannot be obtained from unilateral inertial integration alone. The distance recorded by the sensors represents the instantaneous sensor-to-target range and is subsequently combined with the estimated position and orientation of the instrumented foot within the geometrical reconstruction method.

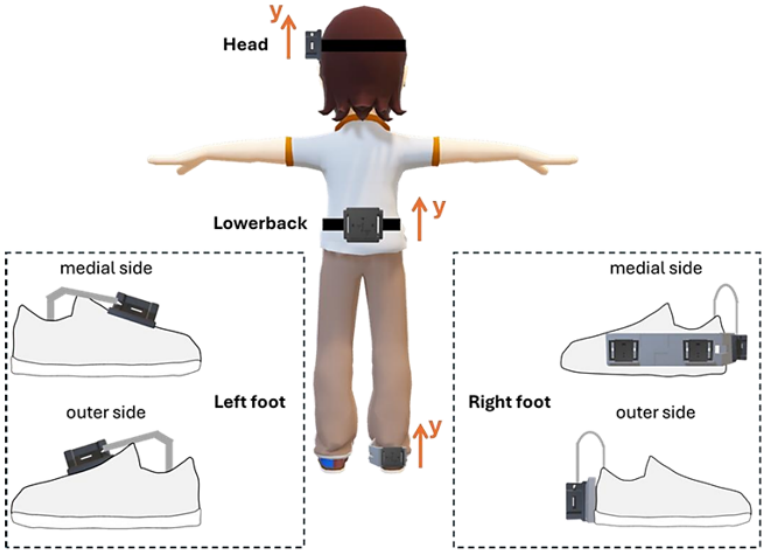



**Figure 3.3:** Complete laboratory configuration of the INDIP wearable system.The sensor orientation is indicated by the local $y$-axis.

The distance-sensing modules were based on the VL6180X infrared time-of-flight sensor (STMicroelectronics). Each device integrates an infrared emitter and receiver and provides short-range distance measurements over an approximately 0–200 mm operating range. Distance data were acquired at 50 Hz. As described in the original wearable method, these signals can subsequently be calibrated and resampled to match the temporal resolution of the magneto-inertial data [2].

Two instrumented pressure insoles were placed inside the participant's shoes. The insoles contained multiple force-sensitive regions distributed across the plantar surface and provided information about foot–ground contact. Their signals were used to support the identification of stance and swing periods and the temporal segmentation of consecutive gait cycles. Since foot-contact information is measured directly, pressure sensing provides a useful complement to inertial gait-event detection, particularly when gait patterns differ from those typically observed in healthy straight walking.

The combination of the three sensing modalities is particularly relevant to the estimation of spatial gait parameters. Together, these signals enable the position and orientation of consecutive footprints to be reconstructed and form the basis of the stride-width estimation method investigated in the present work.

### 3.2.2 Stereophotogrammetric reference system

A stereophotogrammetric motion-capture system was used as the laboratory reference for the validation of the wearable stride-width estimates. The system tracked retro-reflective markers positioned on the participant and on selected components of the wearable setup. Multiple infrared cameras surrounding the acquisition volume recorded the two-dimensional projections of the markers, from which their three-dimensional trajectories were reconstructed within the calibrated laboratory reference frame.

The exact camera configuration differed according to the acquisition centre. Healthy participants were assessed at the PoliTOBIOMed Laboratory of Politecnico di Torino using a 12-camera Vicon system with Vero cameras. The post-stroke participants were assessed at the Lake Lucerne Institute using a 16-camera Vicon configuration, whereas the participants with Parkinson's disease were assessed at the IRCCS Istituto Auxologico Italiano in Piancavallo using a 6-camera Vicon system. Despite the differences in the number of cameras, all systems were configured to provide three-dimensional marker trajectories covering the walking volume required by the corresponding experimental protocol.

For the healthy-control acquisitions, marker trajectories were sampled at 100 Hz and reconstructed using the Vicon Nexus software. The same software environment was used for the processing and reconstruction of the pathological datasets. Before each experimental session, the stereophotogrammetric system was calibrated over the acquisition volume to define the laboratory reference frame and determine the geometrical relationships among the cameras.

Marker placement was adapted to the acquisition protocol and therefore differed between the healthy, Parkinson and post-stroke datasets. For the healthy-control dataset, a total of 39 retro-reflective markers were used. 13 markers were temporary and were applied only during the static acquisition to characterise the geometrical relationship between the feet, the wearable system, and the laboratory reference frame. The remaining 26 markers were retained during the dynamic trials.

Particular attention was given to the marker configuration on the feet, since foot position and orientation were directly involved in the estimation of SW. The markers RHEE and LHEE identified the right and left heel regions, respectively, whereas RTOE and LTOE provided corresponding anterior foot landmarks. Additional dynamic markers were positioned on the rear portion of the shoes and on the wearable system to support the reconstruction of foot orientation and to establish

the geometrical relationship between the optical and wearable measurements.

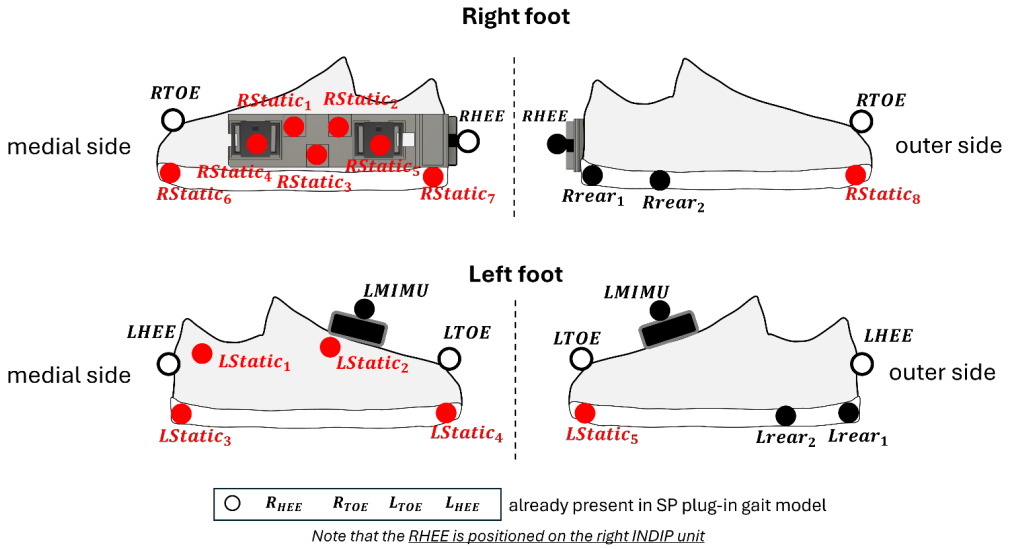



**Figure 3.4:** Foot-marker configuration used for the stereophotogrammetric acquisitions. The additional static markers placed on the shoes and on the right-foot wearable support were used during the static acquisition to characterise the geometry of the feet and wearable system, whereas the remaining markers were retained during the dynamic trials.

Within the dynamic marker set, 16 markers corresponded to the lower-limb Plug-in Gait model and were positioned on anatomical landmarks of the pelvis and lower limbs. These included bilateral markers located at the pelvis, thighs, knees, shanks, ankles, heels, and forefeet, providing the anatomical basis for the stereophotogrammetric reconstruction of lower-limb motion. The Plug-in Gait configuration is shown in Figure 3.5.

The remaining dynamic markers complemented the Plug-in Gait model by tracking the wearable system and additional foot- and pelvis-related reference points. The same general 39-marker configuration was adopted for the participants with Parkinson's disease.

A different full-body marker set was used for the pPS group. In this configuration, 43 markers were applied during the experimental acquisitions. 25 markers corresponded to the dynamic set used for the Parkinson protocol, excluding the head marker, whereas 18 additional markers were introduced to provide a more detailed representation of the trunk, pelvis, lower limbs, and feet.

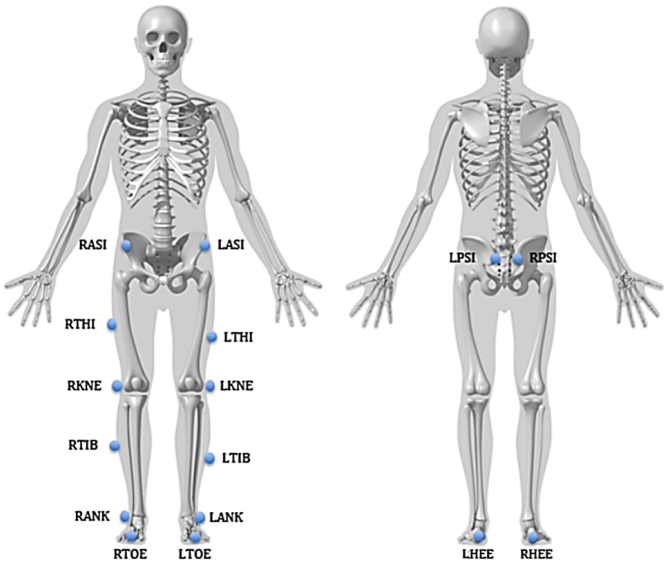



**Figure 3.5:** Lower-limb Plug-in Gait marker set used as the anatomical basis for the stereophotogrammetric reconstruction. Retro-reflective markers are positioned on landmarks of the pelvis, thighs, knees, shanks, ankles, heels, and forefeet.

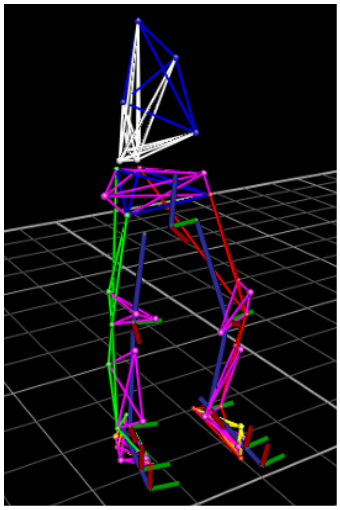


**Figure 3.6:** Three-dimensional reconstruction of the full-body stereophotogrammetric marker set used for the post-stroke participants.

Although the overall marker configurations differed between the parent studies, the foot markers required to derive the reference stride width were available in all datasets. In particular, the heel markers were used to define the reference mediolateral separation between consecutive ipsilateral footprints, while the remaining foot

markers supported the reconstruction of foot orientation and the local direction of progression.

## 3.3 Experimental protocol

The experimental datasets analysed in the present study originated from different parent protocols and acquisition centers. Although the complete experimental batteries included several motor tasks, the present analysis was restricted to two dynamic walking conditions: straight walking at different self-selected speeds and the Two-Minute Walk Test (2MWT). These tasks were selected because they allowed the performance of the stride-width estimation method to be investigated under complementary locomotor conditions. Straight walking provided controlled linear trajectories over a range of gait speeds, whereas the 2MWT included both straight progression and repeated changes in walking direction.

Before the dynamic walking tasks, a series of preliminary acquisitions was performed to verify the correct operation of the wearable system and to obtain the information required for sensor calibration and data personalisation. The exact acquisition sequence depended on the parent-study protocol, but the general procedure was consistent with that adopted in the previous methodological work [8].

### 3.3.1 Preliminary acquisitions

Before instrumenting the participant, the INDIP units underwent a static quality check. The inertial modules were placed on a stable horizontal surface and a static acquisition of at least 60 s was recorded. This procedure was used to verify sensor operation under stationary conditions and to provide data suitable for the subsequent evaluation and compensation of sensor offsets.

Once the participant had been instrumented with the wearable and stereophotogrammetric systems, a standing acquisition was performed. Participants were instructed to remain upright and as still as possible for approximately 10 s. In addition to providing a stationary interval with the sensors worn in their experimental configuration, this acquisition allowed the geometrical relationships between the wearable system, the foot-related marker sets, and the stereophotogrammetric laboratory frame to be characterised.

A dedicated data-personalisation trial was subsequently performed. This procedure was required to determine participant-specific geometrical quantities used by the wearable processing method and to initialise the relationships between the instrumented and contralateral feet. Two versions of the personalisation procedure were available: a standing version and a seated version. The standing version was adopted whenever the participant could comfortably maintain the required

single-support positions; otherwise, the seated version was used to preserve participant safety and allow completion of the procedure. In the standing version, the right foot was initially positioned on a predefined footprint while a reference target was placed at a known location with respect to the infrared distance sensors. After an initial stationary period, the reference objects were removed and the participant remained standing in double support. Participants were then asked to lift the left foot for approximately 10 s, thereby maintaining single support on the instrumented right foot, return to double support, and subsequently lift the right foot for approximately 10 s to obtain the corresponding single-support condition on the left side. The trial concluded with a short predefined walking trajectory including a change in direction.

The main phases of the data-personalisation procedure are illustrated in Figure 3.7.

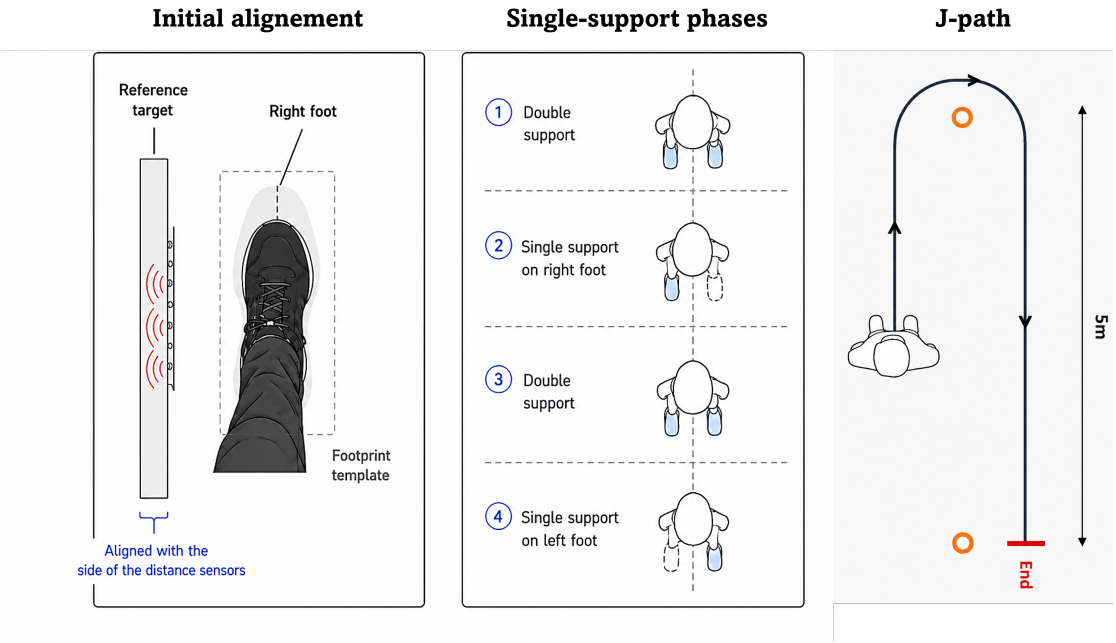



**Figure 3.7:** Schematic representation of the standing data-personalisation procedure. The right foot is initially aligned with a predefined footprint template while a reference target is positioned at a known location with respect to the distance sensors. The protocol then includes alternating double- and single-support phases, followed by a predefined 5-m walking trajectory with a change in direction.

### 3.3.2 Straight walking

Straight walking was used to investigate stride-width estimation during approximately steady linear locomotion and to assess the influence of walking speed.

Participants were instructed to walk along a straight level walkway under three self-selected speed conditions: comfortable, slow, and fast. In the comfortable condition, participants walked at their natural self-selected pace. In the slow condition, they were asked to walk deliberately slower than their preferred speed, whereas in the fast condition they were instructed to walk faster while maintaining a safe and comfortable gait.

The three parent datasets followed the same general three-speed paradigm, although the exact walkway geometry reflected the corresponding acquisition protocol. The HC dataset followed the protocol described by Cicalò [8], in which participants walked along a 5-m straight path. Two trials were acquired for each speed condition, with the walking direction reversed between repetitions. The MOVEWISE protocol adopted for the pwPD group similarly included two repetitions at comfortable, slow, and fast speeds, with a nominal straight-walking distance of 6 m. The GaitCAP protocol used for the pPS group also included preferred, slow, and fast walking conditions, performed along a 10-m straight walkway.

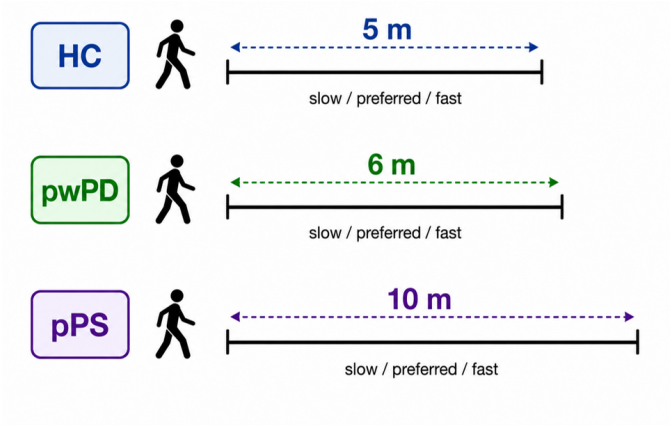



**Figure 3.8:** Schematic comparison of the straight-walking protocols adopted in the three study groups.

The use of self-selected relative speed conditions, rather than externally imposed absolute velocities, allowed the task difficulty to be adapted to the functional capabilities of each participant. This aspect was particularly important for the neurological groups, for whom the absolute walking speed and the ability to safely perform a fast condition could differ substantially from those of the healthy participants. When a requested speed condition could not be completed safely, only the available valid trials were retained.

For the analyses performed in this thesis, individual valid strides obtained during the straight portions of these trials were considered as *straight-walking* observations.

The measured walking speed associated with each stride was subsequently used as a continuous explanatory variable in the statistical analysis, rather than relying exclusively on the nominal slow/preferred/fast task labels.

### 3.3.3 Two-Minutes Walking Test

The second dynamic condition considered in the present work was the 2-Minutes Walking Test (2MWT). During this task, participants were instructed to walk continuously for 2 min at a comfortable self-selected speed along a closed course comprising approximately straight sections connected by repeated changes in direction.

Although the exact pathway geometry differed slightly across the parent protocols, the functional structure of the task was comparable among the three groups. This made the 2MWT particularly relevant to the present study, as it allowed the wearable method to be evaluated not only during linear progression but also during curvilinear walking, extending the assessment beyond the straight-walking conditions in which previous versions of the method had primarily been validated.

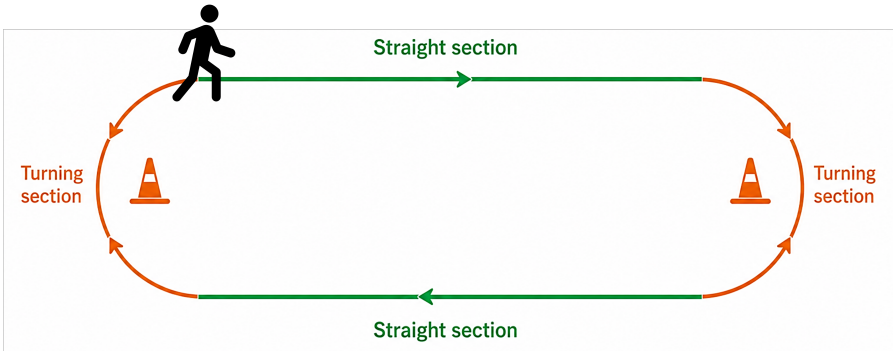



**Figure 3.9:** Schematic representation of the 2MWT pathway and of the locomotor conditions considered in the present analysis. Arrows indicate the direction of progression.

For subsequent processing, the 2MWT recordings were separated into straight-walking and turning portions according to the participant trajectory.

## 3.4 Data processing and stride-width estimation

### 3.4.1 Calibration and data personalisation

Calibration and data personalisation represented a preliminary step of the wearable processing pipeline. Their purpose was to account for sensor-specific measurement

errors and for the geometrical relationship between the foot-mounted sensing system and the participant's foot. In particular, an accurate estimate of the relative orientation between the right-foot wearable support and the longitudinal direction of the foot was required before the distance-sensor measurements could be used for the reconstruction of the contralateral foot.

The calibration procedure adopted in the present work was based on the refined method introduced by Cicalò [8], which extended the original approach proposed by Rossanigo et al. [2]. The updated procedure was developed specifically for the more compact L-shaped right-foot support described in Section 3.2.1. Since the new support introduced small geometrical deviations from an ideal rigid alignment, sensor-specific distance corrections and an additional angular calibration were required.

For most acquisitions, the calibration angle was estimated directly from the distance-sensor measurements recorded during the data-personalisation trial. However, in a subset of the clinical acquisitions, valid distance measurements were not available during this preliminary trial. In these cases, the standard distance-based procedure could not be applied. To avoid excluding otherwise valid walking recordings, an alternative stereophotogrammetry-based calibration was therefore implemented.

Representative examples of usable and unusable distance-sensor recordings during data personalisation are shown in Figure 3.10.

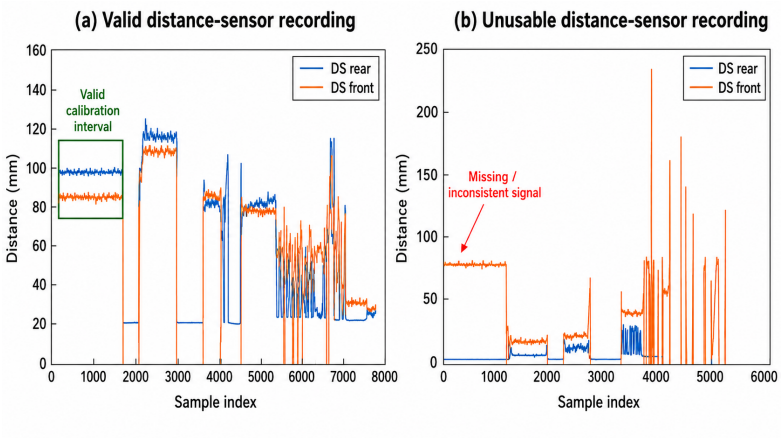



**Figure 3.10:** Examples of distance-sensor recordings acquired during the data-personalisation procedure. (a) Valid acquisition, in which both DS rear and DS front provide stable and consistent measurements over the calibration interval, allowing the standard distance-based calibration to be performed. (b) Representative unusable acquisition, characterised by missing or inconsistent distance information during the initial portion of the trial, preventing application of the standard calibration procedure.

Both approaches yielded the same final quantity, denoted as $\alpha_{\text{calib}}$, which was subsequently used to define the rotation matrix required by the wearable processing pipeline.

### Standard distance-based calibration

The standard procedure relied on the initial static portion of the data-personalisation trial, during which the right foot was aligned with the predefined footprint template and a planar reference target was positioned beside the two infrared distance sensors. The position of the target was defined so that differences between the measurements of the rear and front sensors could be related to the residual angular misalignment of the wearable support with respect to the longitudinal direction of the foot.

Each distance sensor was characterised by a linear calibration model defined by a slope $a_i$ and an offset $b_i$, with $i \in \{\text{rear}, \text{front}\}$. The stored sensor readings were first mapped according to

$$d_i^{\text{raw}} = \frac{d_i^{\text{meas}} - b_i}{a_i}, \tag{3.1}$$

where $d_i^{\text{meas}}$ is the recorded distance value and $d_i^{\text{raw}}$ is the corresponding reconstructed sensor reading.

Empirical sensor-specific offsets, determined at a reference distance of 10 cm, were subsequently applied:

$$d_i^{\text{off}} = d_i^{\text{raw}} + o_i, \tag{3.2}$$

where $o_i$ represents the offset correction associated with the corresponding distance sensor.

A stationary interval within the initial phase of the data-personalisation trial was selected and the corrected distance measurements were averaged over this interval. For the rear sensor, the resulting mean value was directly retained as

$$d_{\text{rear}}^{\text{corr}} = \overline{d_{\text{rear}}^{\text{off}}}. \tag{3.3}$$

The front sensor required an additional correction to account for the geometrical deflection of the support. Two parameters previously determined from the physical geometry of the right-foot setup were used: $\beta_{\text{defl}}$, representing the angular deflection of the front sensor, and $\beta_{\text{shift}}$, representing the corresponding linear displacement. The corrected front distance was therefore calculated as

$$d_{\text{front}}^{\text{corr}} = \overline{d_{\text{front}}^{\text{off}}} \cos\left(\beta_{\text{defl}}\right) + \beta_{\text{shift}}. \tag{3.4}$$

Once the two corrected distances were available, the calibration angle was estimated from the geometrical relationship between their difference and the known distance $L_{\mathrm{DS}}$ between the rear and front distance sensors:

$$\alpha_{\mathrm{calib}} = \operatorname{atan2}\left(d_{\mathrm{front}}^{\mathrm{corr}} - d_{\mathrm{rear}}^{\mathrm{corr}}, L_{\mathrm{DS}}\right). \tag{3.5}$$

The resulting angle represents the in-plane rotational correction required to align the wearable sensing geometry with the longitudinal direction used for foot reconstruction. It was subsequently used to define the calibration rotation matrix

$$\mathbf{R}_{\mathrm{calib}} = \begin{bmatrix} \cos\alpha_{\mathrm{calib}} & -\sin\alpha_{\mathrm{calib}} & 0 \\ \sin\alpha_{\mathrm{calib}} & \cos\alpha_{\mathrm{calib}} & 0 \\ 0 & 0 & 1 \end{bmatrix}. \tag{3.6}$$

The relative positions of the rear and front distance sensors with respect to the foot-mounted inertial unit were then rotated using $\mathbf{R}_{\mathrm{calib}}$. These corrected sensor positions were retained for the subsequent reconstruction of the contralateral foot.

### Alternative marker-based calibration

For some pwPD and pPS acquisitions, the distance-sensor signals required by the procedure described above were not available during the data-personalisation trial. Since the corresponding dynamic walking recordings were otherwise suitable for analysis, excluding these participants would have resulted in an unnecessary loss of clinically relevant data. An alternative calibration strategy based on the stereophotogrammetric measurements was therefore introduced.

The alternative procedure exploited the temporary retro-reflective markers placed on the right-foot setup during the static standing acquisition. In particular, two markers were physically positioned in correspondence with the rear and front distance sensors, respectively. Their mean three-dimensional positions during the static acquisition were denoted as $\mathbf{p}_{\mathrm{DS,rear}}$ and $\mathbf{p}_{\mathrm{DS,front}}$. The mean positions of the right heel and toe markers, RHEE and RTOE, were similarly obtained and denoted as $\mathbf{p}_{\mathrm{RHEE}}$ and $\mathbf{p}_{\mathrm{RTOE}}$.

Since the required calibration concerned the orientation of the system in the horizontal plane, only the mediolateral and anteroposterior components of the marker positions were considered. Two directional vectors were then defined. The first represented the longitudinal direction of the right foot:

$$\mathbf{v}_{\mathrm{foot}} = \mathbf{p}_{\mathrm{RTOE}} - \mathbf{p}_{\mathrm{RHEE}}, \tag{3.7}$$

whereas the second represented the direction defined by the two distance sensors on the rigid support:

$$\mathbf{v}_{\mathrm{DS}} = \mathbf{p}_{\mathrm{DS,front}} - \mathbf{p}_{\mathrm{DS,rear}}. \tag{3.8}$$

The marker-based calibration angle was then calculated as the angle between these two vectors:

$$\alpha_{\text{calib}}^{\text{SP}} = \cos^{-1}\left(\frac{\mathbf{v}_{\text{DS}} \cdot \mathbf{v}_{\text{foot}}}{\|\mathbf{v}_{\text{DS}}\| \, \|\mathbf{v}_{\text{foot}}\|}\right). \tag{3.9}$$

This formulation assumes that the relative orientation between the line joining the two distance sensors and the longitudinal foot axis, directly observable from the stereophotogrammetric marker geometry, provides an estimate of the same in-plane misalignment quantified by $\alpha_{\text{calib}}$ in the standard distance-based procedure.

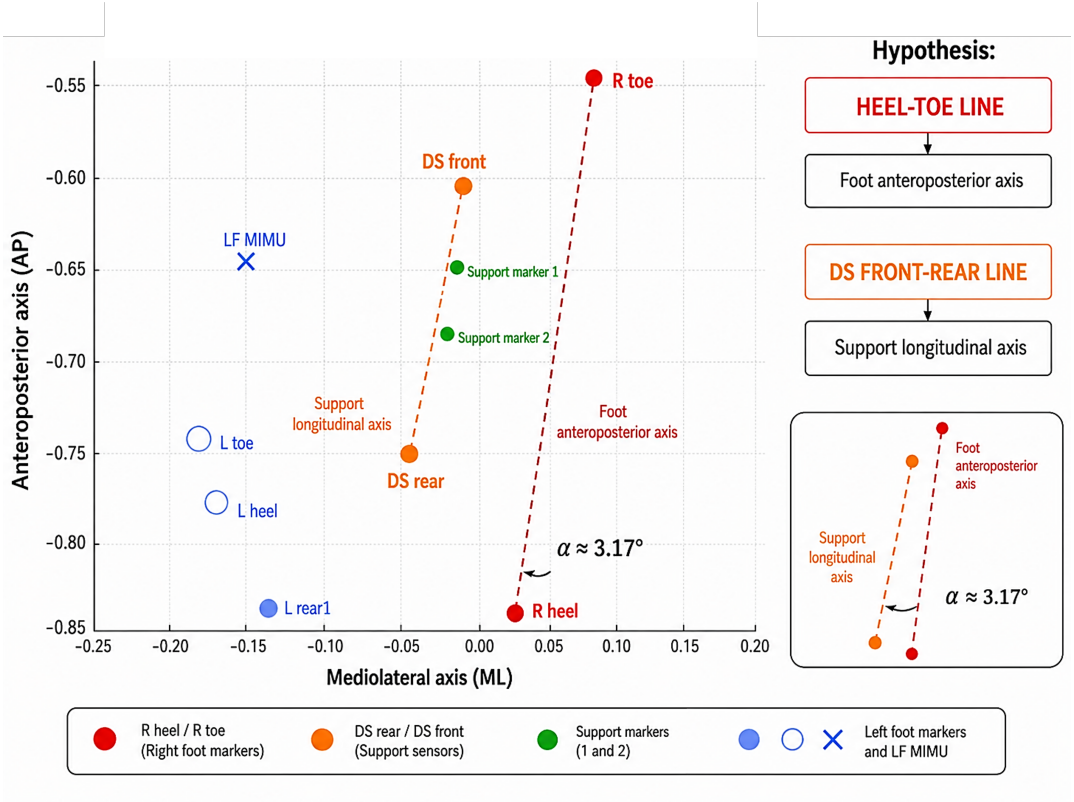



**Figure 3.11:** Stereophotogrammetric reconstruction of the markers during the standing phase used for the alternative marker-based calibration. The foot anteroposterior axis was identified by the heel-to-toe line (R heel–R toe), whereas the support longitudinal axis was identified by the line joining the rear and front distance-sensor markers (DS rear–DS front). The angle $\alpha$ between these two directions was used as an alternative estimate of the calibration angle when valid distance-sensor data were unavailable during data personalisation.

For acquisitions stored with a reversed horizontal reference-frame convention,

the stereophotogrammetric marker coordinates were first reoriented to a common mediolateral–anteroposterior convention before computing the two vectors. The resulting angle was then used in place of the distance-based $\alpha_{\text{calib}}$ to construct the same calibration matrix given in Equation 3.6.

Importantly, the marker-based procedure was used only as a fallback when the distance-based calibration could not be performed. No other modification was introduced downstream: once $\alpha_{\text{calib}}$ had been obtained, the same corrected sensor geometry and the same wearable stride-width estimation pipeline were applied to all participants. This allowed acquisitions with missing distance-sensor data during personalisation to be retained while preserving a common processing framework across the three study populations.

### 3.4.2 Wearable stride-width estimation

The wearable SW estimation procedure was based on the method originally proposed by Rossanigo et al. [2] and subsequently refined by Cicalò [8]. The underlying principle is to combine the trajectory and orientation of the instrumented right foot, obtained from the foot-mounted MIMU, with the measurements provided by the two infrared distance sensors to reconstruct the relative position of the contralateral foot. The same processing framework was applied to the straight-walking and 2MWT trials considered in the present study.

The processing pipeline comprised a sequence of stages including signal preprocessing, gait-event detection, foot-trajectory reconstruction, identification of valid inter-foot scans, reconstruction of the contralateral footprint, and computation of SW.

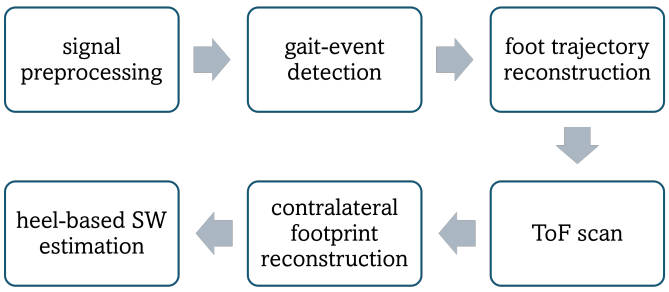



**Figure 3.12:** Overall workflow adopted for wearable stride-width estimation.

The magneto-inertial and plantar-pressure signals were first preprocessed and

expressed in a common biomechanically meaningful reference frame. Gyroscope biases estimated during the preliminary static acquisition were removed before processing. Gait events were then identified separately for the right and left feet by combining information from the pressure insoles and foot-mounted MIMUs. Initial and final contacts were associated to identify stance and swing phases and to segment consecutive strides.

The presence of neurological gait impairments and repeated changes in direction could occasionally make gait-event identification more challenging than during regular straight walking. For this reason, additional event-recovery procedures were applied when the standard detection did not provide a sufficiently consistent sequence of gait events, particularly within curvilinear portions. The selection criteria used in these cases were adapted to the characteristics and quality of the individual recordings rather than applying a single fixed threshold to all participants.

Once gait events had been identified, the trajectory of each foot-mounted MIMU was reconstructed. Zero-velocity updates were applied during the stationary portions of the gait cycle to limit the drift associated with the integration of inertial signals. Consecutive strides and continuous walking periods were then identified from the reconstructed foot trajectories. The lower-back MIMU provided complementary information on changes in walking direction and was used to support the identification of turning portions within the continuous walking sequences.

The subsequent stage focused on the measurements acquired by the two right-foot ToF sensors. A useful inter-foot scan occurs when the instrumented right foot moves past the contralateral foot while the latter is in stance. Candidate scanning intervals were therefore identified by combining the gait phases of the two feet with the availability and consistency of the distance measurements. Short or incomplete measurement sequences that did not provide sufficient information for the subsequent geometrical reconstruction were not considered.

For each valid scanning interval, the positions of the rear and front distance sensors were reconstructed from the estimated position and orientation of the right-foot MIMU and from their calibrated locations on the rigid support. The calibration corrections described in Section 3.4.1 were therefore incorporated before the distance measurements were used for foot reconstruction.

The measured distances were initially expressed along the sensing direction of the corresponding ToF sensor. Using the estimated orientation of the instrumented foot, each measurement was transformed into the common reference frame associated with the local direction of progression. The resulting three-dimensional points represented samples of the medial border of the contralateral left foot during stance.

As in the method described by [8], the detected points were approximated by a linear model representing the medial border of the left foot. Together with the participant-specific shoe length and width, this model was used to estimate the position and orientation of the non-instrumented footprint. The right-foot footprint

was instead reconstructed from the estimated right-foot pose and the known shoe dimensions. In this way, the relative positions of the two feet could be obtained within the same local reference frame.

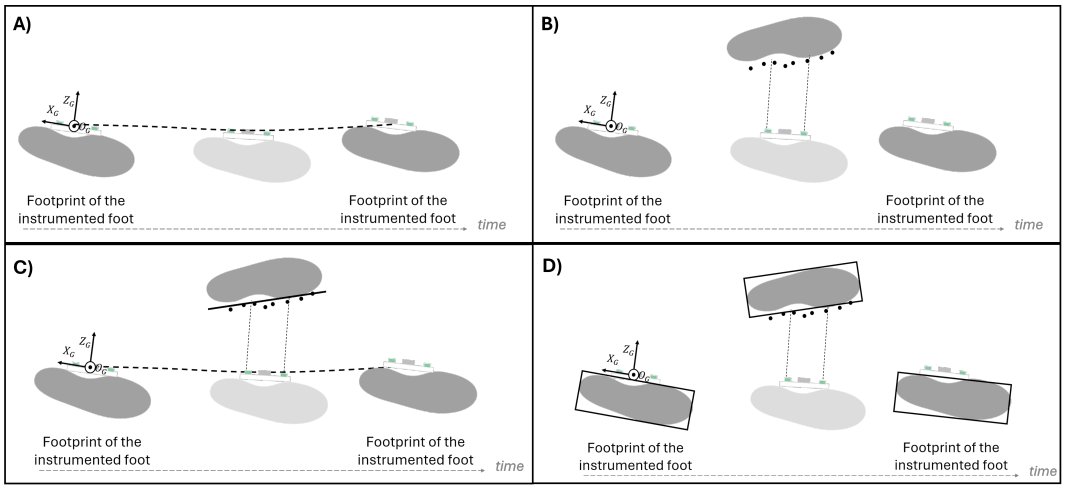



**Figure 3.13:** Schematic representation of the wearable stride-width estimation procedure. A) the instrumented right foot is tracked during progression; B) the two infrared distance sensors scan the medial border of the contralateral foot while it is in stance; C) the detected points are approximated by a linear model; D) consecutive footprints are reconstructed in a common reference frame for the subsequent estimation of stride width. Adapted from [8].

For the calculation of SW, the reconstructed footprints were represented by their heel points rather than by their centroids. The heel point of each footprint was defined as the midpoint of its posterior edge. This definition was applied consistently to both the instrumented and reconstructed contralateral footprints.

For a right-foot stride, two consecutive right heel positions were used to define the local direction of progression. The corresponding right SW was then calculated as the perpendicular distance between the intervening left heel position and the line joining the two consecutive right heel points. The same geometrical definition was applied to the left side using consecutive left heel positions and the corresponding right heel position.

The estimation of left-sided SW required an additional transformation because consecutive left footprints were obtained from different right-foot scanning events. The left footprint reconstructed during the preceding scan was therefore transferred to the reference frame of the current scan by means of a rigid rotation and translation determined from the corresponding right-foot configurations. This allowed consecutive left heel positions to be expressed in the same reference frame before calculating the local direction of progression and the associated SW.

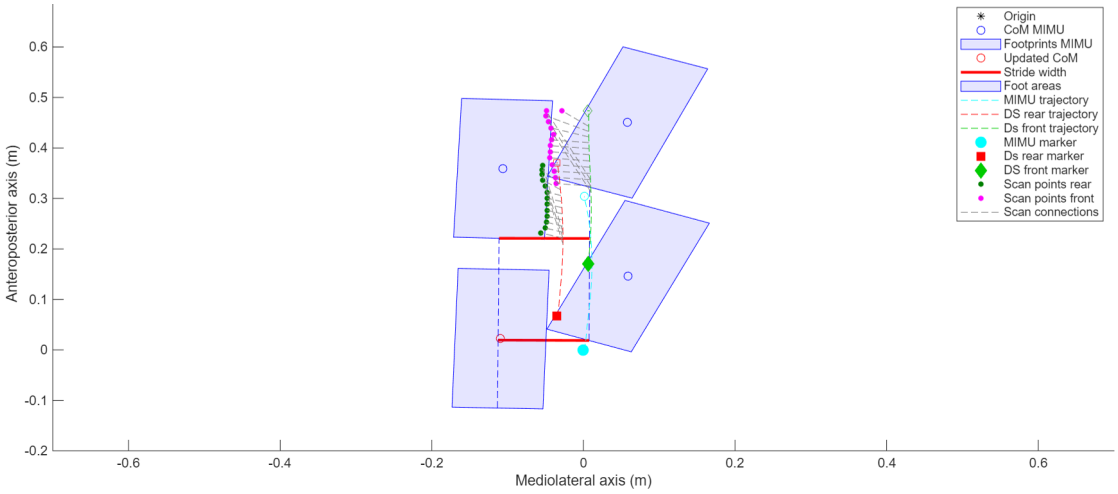



**Figure 3.14:** Representative example of the wearable reconstruction used for heel-based stride-width estimation. The reconstructed footprints are shown together with the right-foot MIMU trajectory, the rear and front time-of-flight sensor trajectories, and the corresponding scan points. Stride width is highlighted in red and represents the perpendicular distance between the contralateral heel point and the local direction of progression defined by consecutive ipsilateral heel positions.

This heel-based and locally defined formulation was used for all wearable SW estimates considered in the present study. Since the direction of progression was determined independently for each pair of consecutive ipsilateral footprints, the definition could be applied both during approximately straight progression and during changes in walking direction. The resulting stride-by-stride wearable estimates were subsequently paired with the corresponding stereophotogrammetric reference measurements for validation.

### 3.4.3 Stereophotogrammetric reference stride width

The stereophotogrammetric measurements were used as the reference for the validation of the wearable SW estimates. Marker trajectories were reconstructed in Vicon Nexus and visually inspected before being exported for subsequent processing. Marker labelling was checked to correct possible misidentifications, while trajectory gaps caused by temporary marker occlusion were reviewed and filled only when a reliable reconstruction could be obtained.

An example of the three-dimensional marker reconstruction within the calibrated laboratory reference frame is shown in Figure 3.15. The static acquisition included additional markers used to characterise the geometry of the feet and of the wearable setup, whereas a reduced marker set was retained during the dynamic walking trials.

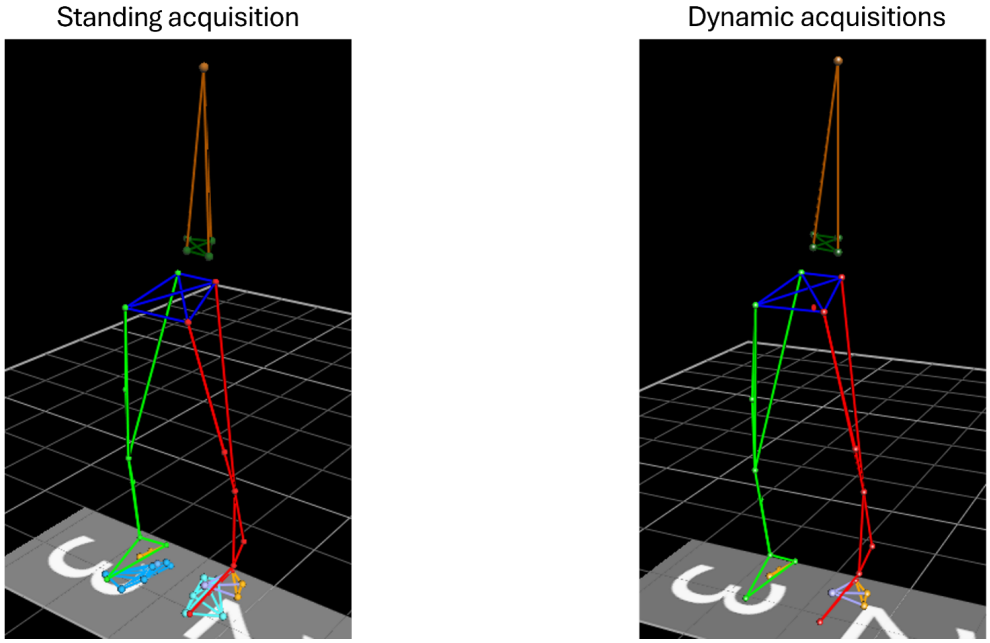



**Figure 3.15:** Example of three-dimensional marker reconstruction within the calibrated stereophotogrammetric laboratory reference frame. The static acquisition includes the additional markers required to characterise the foot and wearable-system geometry, whereas the reduced marker set is retained during dynamic acquisitions.

Among the available markers, RHEE, LHEE, RTOE, and LTOE were particularly relevant to the present analysis, as they provided the main anatomical landmarks required for gait-event identification and for the subsequent calculation of the reference SW.

After export from Vicon Nexus, the marker trajectories were further processed in MATLAB. The trajectories were filtered and converted to metres, and gait events were identified independently from the right- and left-foot heel and toe kinematics. Stable foot-contact instants were subsequently identified and used to associate consecutive ipsilateral and contralateral foot positions.

The stereophotogrammetric reference SW was calculated using the same heel-based geometrical definition adopted for the wearable system. For each stride, two consecutive heel positions of the same foot defined the local direction of progression. The corresponding SW was obtained as the perpendicular distance between the contralateral heel position and this local direction.

For a right-foot stride, the line connecting two consecutive right heel positions therefore defined the local direction of progression, while the perpendicular distance of the intervening left heel from this line provided the reference right SW. The

same procedure was applied symmetrically to the left side using consecutive left heel positions and the corresponding right heel position.

Since the direction of progression was defined locally for each stride rather than with respect to a fixed laboratory axis, the same approach could be applied during both straight walking and changes in direction. This ensured that the stereophotogrammetric and wearable measurements were based on the same heel-based geometrical definition, allowing a direct stride-by-stride comparison between the two systems.

### 3.4.4 Matching and validity criteria

To enable a direct comparison between the wearable and stereophotogrammetric SW estimates, measurements obtained from the two systems were matched stride by stride. The matching procedure was performed separately for the right and left sides and exclusively considered the heel-based SW estimates for all participant groups.

Only measurements belonging to the same experimental test, trial, and processing interval were considered eligible for matching. Within each interval, the correspondence between a stereophotogrammetric stance and an INDIP scan was established on the basis of their temporal proximity. In particular, the mid-stance instant associated with each stereophotogrammetric estimate was compared with the corresponding mid-stance instant identified by the wearable pipeline. A pair was considered temporally matched when the two mid-stance events occurred within a tolerance of ±50 frames, corresponding to ±0.5 s at the 100-Hz sampling frequency. Once a valid correspondence was identified, the associated stereophotogrammetric and INDIP SW values were retained as a matched pair.

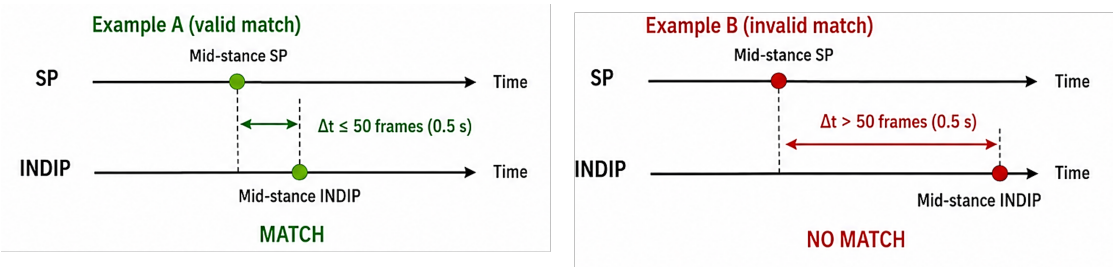



**Figure 3.16:** Schematic representation of the temporal matching between stereophotogrammetric (SP) and INDIP stride-width estimates.

Measurements were excluded when the required processing outputs were not available in both systems, when the corresponding SW value could not be computed, or when missing or non-finite values were present. Additional plausibility checks were applied to remove measurements that were not compatible with a

physiologically meaningful gait pattern. These criteria were used as quality-control procedures rather than as fixed assumptions on the gait characteristics of the different clinical populations.

Following the initial validity checks, the signed error associated with each matched pair was calculated as the difference between the INDIP estimate and the stereophotogrammetric reference. Outliers were subsequently identified from the signed-error distribution using the $1.5 \times$ IQR criterion. Since measurement performance could differ between linear and curvilinear locomotion, outlier detection was performed separately for straight-walking and turning observations. Measurements falling below $Q_1 - 1.5 \times \text{IQR}$ or above $Q_3 + 1.5 \times \text{IQR}$ within the corresponding walking condition were excluded from the final validation dataset.

Each matched estimate also retained the locomotor-condition classification provided by the wearable processing pipeline. Strides labelled as belonging to a turning interval were therefore analysed separately from those performed during straight walking. This classification was subsequently used both for the descriptive analysis of the validation dataset and for the statistical models investigating the effect of walking condition on measurement error.

The resulting set of valid, temporally matched heel-based SW measurements constituted the dataset used for the subsequent validation analyses.

## 3.5 Statistical analysis

Statistical analyses were performed in MATLAB. The significance level was set at $\alpha = 0.05$. Descriptive statistics were selected according to the type and distribution of the analysed variables. Stride velocity, reference stride width, and absolute stride-width estimation error were summarised using median and interquartile range where appropriate.

Differences in stride velocity and stereophotogrammetric reference stride width across populations and walking conditions were investigated using linear mixed-effects models. Population (HC, pPS, pwPD), walking condition (straight, turning), and their interaction were included as fixed effects, while participant identity was included as a random intercept to account for repeated observations within subjects. When significant effects or interactions were identified, pairwise comparisons were performed and the resulting $p$-values were adjusted for multiple comparisons using the Holm procedure.

Absolute stride-width estimation error was defined as the absolute difference between the INDIP and stereophotogrammetric estimates. The effects of population, walking condition, and their interaction on absolute error were assessed using a linear mixed-effects model with participant identity included as a random intercept. Condition effects were subsequently examined within each population.

Agreement between the wearable and stereophotogrammetric estimates was evaluated at subject level using Bland–Altman analysis. For each participant and walking condition, the mean INDIP–reference difference was calculated together with the corresponding mean stride width. Bias was defined as the mean INDIP–reference difference, and 95% limits of agreement were calculated as the bias $\pm 1.96$ standard deviations of the subject-level differences.

The association between wearable and reference stride-width estimates was assessed using Pearson's correlation coefficient separately for each population and walking condition. Correlations were first calculated using the original stride-level measurements. A second analysis was performed after subtracting the subject- and condition-specific mean from both the reference and wearable measurements, thereby removing between-subject differences in mean stride width and focusing on within-subject covariation. Confidence intervals for stride-level correlations were estimated using bootstrap resampling at subject level in order to preserve the clustered structure of repeated strides within participants.

Measurement sensitivity was assessed through the minimal detectable change at the 95% confidence level ($MDC_{95}$). $MDC_{95}$ was estimated separately for straight walking and turning. For clinical interpretation in pwPD, the straight-walking $MDC_{95}$ was compared with the minimally important difference for stride width previously reported in the literature.

Participant-reported comfort, safety, and perceived gait alteration were analysed descriptively and expressed as percentages of questionnaire respondents within each population. Finally, the freezing-of-gait analysis was exploratory and descriptive and did not involve inferential statistical testing.

# Chapter 4

# Results

## 4.1 Dataset overview

All 30 participants included in the study contributed valid stereophotogrammetric–wearable SW pairs to the final validation dataset: 18 HCs, 6 pPSs, and 6 pwPDs.

Following stride-by-stride temporal matching between the INDIP and stereophotogrammetric measurements and the initial validity checks described in Section 3.4.4, a total of 4,565 matched heel-based SW estimates were available for analysis. Outliers were subsequently identified from the signed SW error separately for straight walking and turning using the $1.5 \times$ IQR criterion. Overall, 52 observations were excluded at this stage, corresponding to 1.1% of the matched estimates.

The final validation dataset therefore comprised 4,513 valid heel-based SW estimates. Of these, 2,679 were obtained from HCs, 1,098 from pPSs, and 736 from pwPDs. Regarding walking condition, 2,571 estimates were classified as straight walking and 1,942 as turning. The distribution of the retained measurements across populations and walking conditions is reported in Table 4.1.

**Table 4.1:** Distribution of matched heel-based stride-width estimates across populations and walking conditions. The number of estimates before and after outlier removal is also reported.

| Population | Participants | Matched | Removed | Straight | Turning | Final |
|---|---|---|---|---|---|---|
| HC | 18 | 2707 | 28 | 1104 | 1575 | 2679 |
| pPS | 6 | 1118 | 20 | 852 | 246 | 1098 |
| pwPD | 6 | 740 | 4 | 615 | 121 | 736 |
| **Total** | **30** | **4565** | **52** | **2571** | **1942** | **4513** |

## 4.2 Gait characteristics across populations and walking conditions

Gait characteristics were examined in terms of stride velocity and stereophotogrammetric reference SW. Stride velocity was available for 4,484 of the 4,513 retained SW observations, whereas a valid reference SW was available for all observations. Turning observations were available for all HCs and pPSs, whereas only 4 of the 6 pwPDs contributed valid turning data.

**Table 4.2:** Stride velocity and stereophotogrammetric reference stride width across populations and walking conditions. Values are reported as median [interquartile range].

| Variable | Population | Straight | Turning |
|---|---|---|---|
| Stride velocity [m/s] | HC | 0.958 [0.812–1.115] | 0.846 [0.667–1.010] |
| | pPS | 0.871 [0.727–1.015] | 0.798 [0.665–0.952] |
| | pwPD | 0.346 [0.235–0.450] | 0.262 [0.190–0.371] |
| Reference SW [m] | HC | 0.122 [0.092–0.155] | 0.187 [0.119–0.292] |
| | pPS | 0.141 [0.118–0.166] | 0.189 [0.114–0.258] |
| | pwPD | 0.093 [0.084–0.113] | 0.087 [0.073–0.106] |

### Stride velocity

Stride velocity differed across populations and walking conditions (Figure 4.1).

During straight walking, the median stride velocity was 0.958 m/s in HCs, 0.871 m/s in pPSs, and 0.346 m/s in pwPDs. During turning, the corresponding median values were 0.846, 0.798, and 0.262 m/s, respectively.

The linear mixed-effects model showed significant effects of population ($F = 43.42$, $p < 0.001$), walking condition ($F = 469.12$, $p < 0.001$), and their interaction ($F = 12.77$, $p < 0.001$) on stride velocity.

Pairwise comparisons showed no significant difference between HCs and pPSs during either straight walking ($p_{\text{Holm}} = 0.304$) or turning ($p_{\text{Holm}} = 0.626$). In contrast, pwPDs walked significantly more slowly than both HCs and pPSs in both conditions ($p_{\text{Holm}} < 0.001$ for all comparisons). Within each population, stride velocity was significantly lower during turning than during straight walking. The estimated turning-minus-straight differences were $-0.162$ m/s for HCs, $-0.086$ m/s for pPSs, and $-0.122$ m/s for pwPDs, with all comparisons remaining significant after Holm correction ($p_{\text{Holm}} < 0.001$).

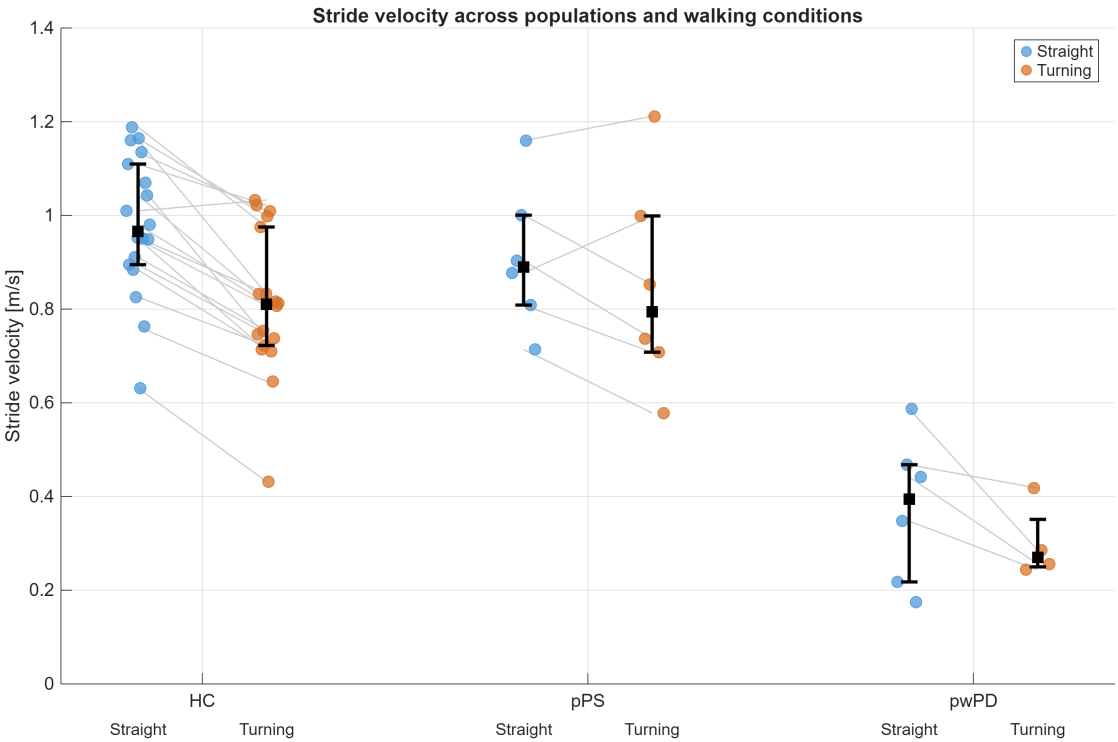



**Figure 4.1:** Subject-level stride velocity across populations and walking conditions. Each point represents the median stride velocity of one participant within the corresponding condition. Grey lines connect straight-walking and turning values from the same participant when both conditions were available. Black squares represent the group median and error bars indicate the interquartile range.

## Reference stride width

The stereophotogrammetric reference SW also differed according to population and walking condition (Figure 4.2).

During straight walking, the median reference SW was 0.122 m in HCs, 0.141 m in pPSs, and 0.093 m in pwPDs. During turning, the corresponding values were 0.187, 0.189, and 0.087 m, respectively.

The linear mixed-effects model identified significant effects of population ($F = 6.82$, $p = 0.001$), walking condition ($F = 666.09$, $p < 0.001$), and the population-by-condition interaction ($F = 59.67$, $p < 0.001$).

During straight walking, no significant difference in reference SW was observed between HCs and pPSs ($p_{\text{Holm}} = 0.448$). pwPDs, however, showed a significantly narrower reference SW than both HCs ($p_{\text{Holm}} = 0.014$) and pPSs ($p_{\text{Holm}} = 0.007$).

During turning, reference SW differed significantly among all three populations. Compared with HCs, pPSs showed a lower reference SW ($p_{\text{Holm}} = 0.011$), while

pwPDs showed markedly lower values than both HCs and pPSs ($p_{\text{Holm}} < 0.001$).

Within-population comparisons showed an increase in reference SW during turning in both HCs and pPSs. The estimated turning-minus-straight differences were 0.073 m and 0.049 m, respectively ($p_{\text{Holm}} < 0.001$ for both). Conversely, pwPDs showed a small but significant reduction in reference SW during turning, with an estimated difference of −0.013 m ($p_{\text{Holm}} < 0.001$).

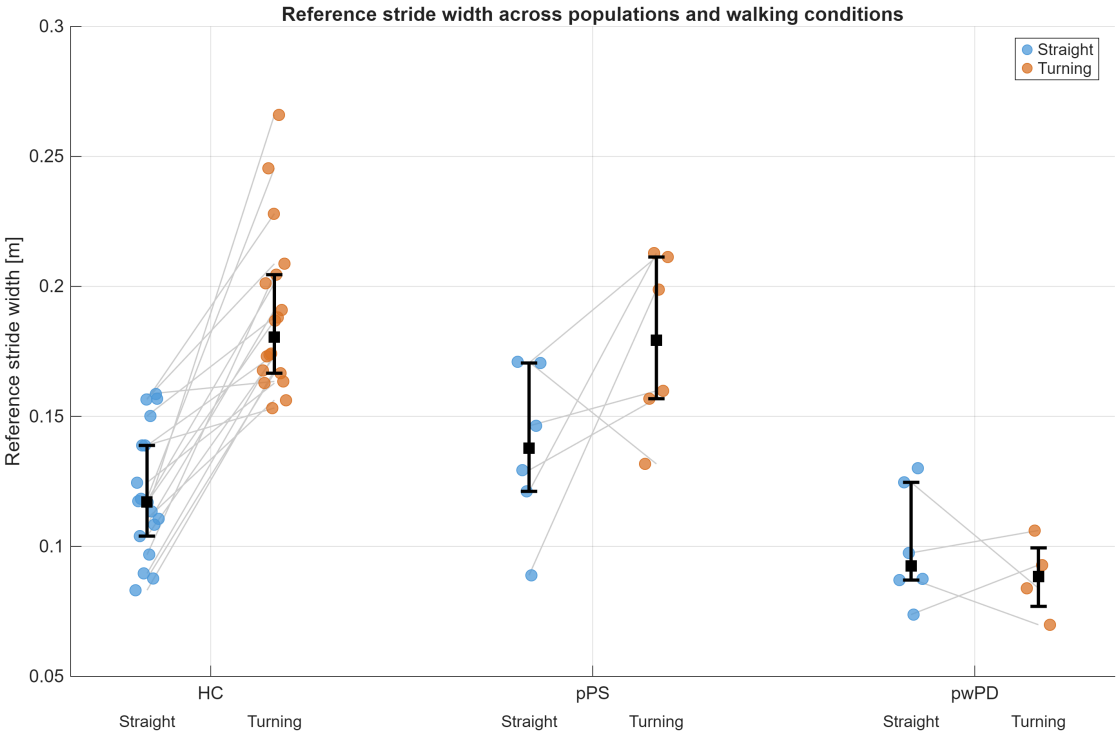



**Figure 4.2:** Subject-level stereophotogrammetric reference stride width across populations and walking conditions. Each point represents the median reference stride width of one participant within the corresponding condition. Grey lines connect straight-walking and turning values from the same participant when both conditions were available. Black squares represent the group median and error bars indicate the interquartile range.

## 4.3 Stride-width estimation performance

### Absolute stride-width estimation error

The absolute SW estimation error was examined across populations and walking conditions to evaluate whether measurement performance differed between healthy participants and the two clinical groups, and whether turning introduced an

additional source of error.

Across all population–condition combinations, median absolute errors ranged from approximately 0.018 to 0.040 m (1.8–4.0 cm). Overall, the magnitude of the estimation error was comparable across HCs, pPSs, and pwPDs, and no significant main effect of population was detected. Thus, the presence of a pathological gait pattern was not associated with a systematic increase in SW estimation error.

The effect of walking condition differed across populations. In HCs, absolute error was significantly greater during turning than during straight walking ($p < 0.001$). Conversely, no significant difference between straight walking and turning was observed in either pPSs or pwPDs. Accordingly, the increase in estimation error associated with turning was evident in the healthy group, whereas no significant condition-related increase was detected in the two pathological populations.

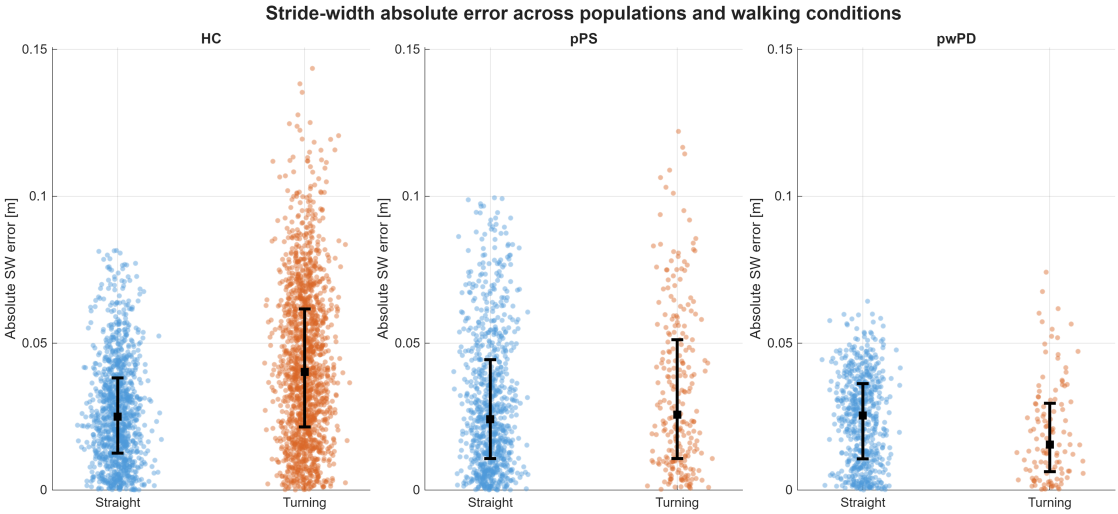



**Figure 4.3:** Absolute stride-width estimation error across populations and walking conditions. Individual observations are shown separately for straight walking and turning. Black markers and error bars indicate the corresponding distribution summary. Turning was associated with a significantly greater absolute error in healthy controls, whereas no significant difference between walking conditions was observed in post-stroke participants or participants with Parkinson's disease. *** $p < 0.001$; n.s., not significant.

## Minimum detectable change

Measurement sensitivity was further evaluated in pwPDs during straight walking by estimating the 95% minimum detectable change ($MDC_{95}$). The resulting $MDC_{95}$ was approximately 0.020 m (2.0 cm).

This value was close in magnitude to the minimum clinically important difference

(MCID) of 1.82 cm previously reported for stride width in Parkinson's disease [45]. Therefore, the change required to exceed expected measurement variability was of the same order of magnitude as the previously reported clinically relevant change in SW.

## Subject-level agreement between INDIP and the reference system

Agreement between INDIP and stereophotogrammetric SW measurements was subsequently examined at subject level using Bland–Altman analysis (Figure 4.4). For each participant and walking condition, the mean difference between the wearable and reference estimates was plotted against the corresponding mean SW. The difference was defined as INDIP minus stereophotogrammetric SW, such that positive values indicate larger estimates obtained with INDIP.

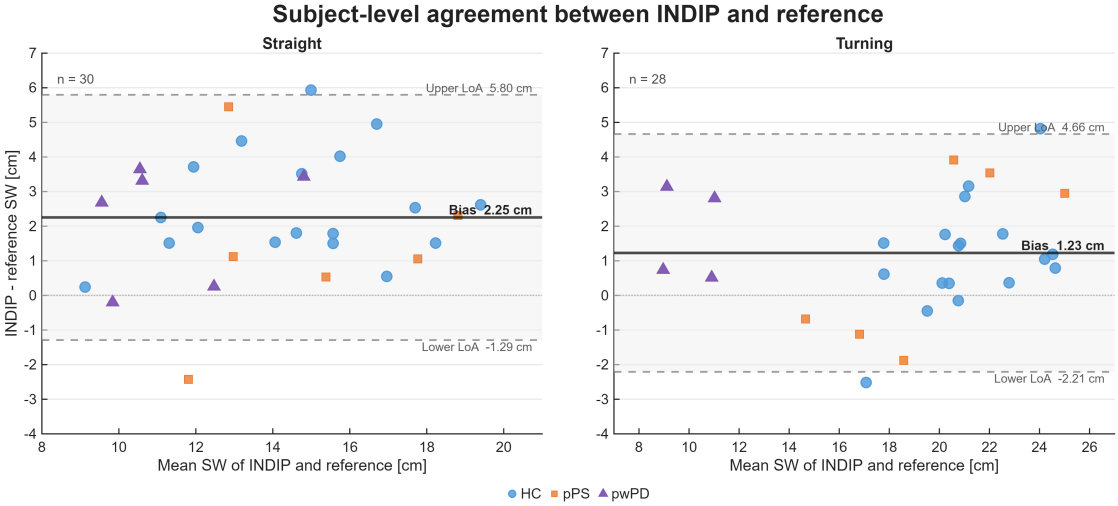



**Figure 4.4:** Subject-level Bland–Altman analysis of INDIP and stereophotogrammetric stride-width estimates during straight walking (left) and turning (right). Each point represents one participant and is positioned according to the participant-specific mean stride width and mean INDIP–reference difference. The solid horizontal line represents the mean bias, while dashed lines indicate the 95% limits of agreement. Positive differences indicate larger stride-width estimates obtained with INDIP than with the stereophotogrammetric reference.

During straight walking, data were available for all 30 participants. A positive mean bias of 2.25 cm was observed, with 95% limits of agreement ranging from −1.29 to 5.80 cm. During turning, 28 participants contributed valid data, as turning measurements were not available for two of the six pwPDs. The mean bias

remained positive but was lower, at 1.23 cm, with 95% limits of agreement ranging from −2.21 to 4.66 cm.

Thus, at subject level, INDIP showed a positive average bias in both walking conditions, corresponding to a tendency to provide larger SW estimates than the stereophotogrammetric reference. However, the dispersion of the subject-level differences and the width of the limits of agreement indicated substantial inter-subject variability in absolute agreement, with some participants showing considerably larger measurement differences than others.

## 4.4 Association between wearable and reference stride-width estimates

Given the inter-subject variability observed in the Bland–Altman analysis, the association between wearable and reference estimates was further examined to distinguish between differences in absolute measurement level across participants and the ability of the system to track stride-to-stride changes within each participant. The association between stereophotogrammetric and INDIP SW estimates was evaluated separately for each population and walking condition. Two complementary stride-level analyses were considered. First, Pearson correlations were calculated from the original, untransformed measurements. These raw correlations capture both differences in mean SW between participants and stride-to-stride variations within participants. A second analysis was then performed after centering both reference and wearable measurements within each subject and walking condition. This removed between-subject differences in mean SW and allowed the association between within-subject deviations from each participant's own mean value to be examined separately.

### Raw stride-level association

Using the original stride-level measurements, positive associations between reference and wearable SW were observed in all populations and walking conditions (Figure 4.5).

In HCs, the association was strong during both straight walking and turning. During straight walking, the correlation coefficient was $r = 0.89$ (95% CI [0.87–0.91]), whereas during turning it increased to $r = 0.93$ (95% CI [0.90–0.95]).

A similar pattern was observed in pPSs, although the association differed more markedly between walking conditions. During straight walking, reference and wearable estimates were strongly correlated ($r = 0.88$, 95% CI [0.83–0.93]). During turning, the association remained positive but was lower, with $r = 0.73$ (95% CI [0.59–0.78]).

Lower raw correlations were observed in pwPDs. The correlation coefficient was $r = 0.63$ during straight walking (95% CI [0.35–0.78]) and $r = 0.51$ during turning (95% CI [0.25–0.86]). The confidence interval was particularly wide for turning, consistent with the smaller number of participants contributing turning observations in this population.

Overall, the raw stride-level analysis therefore showed a strong association between reference and wearable estimates in HCs and pPSs, particularly during straight walking, while more moderate associations were observed in pwPDs.

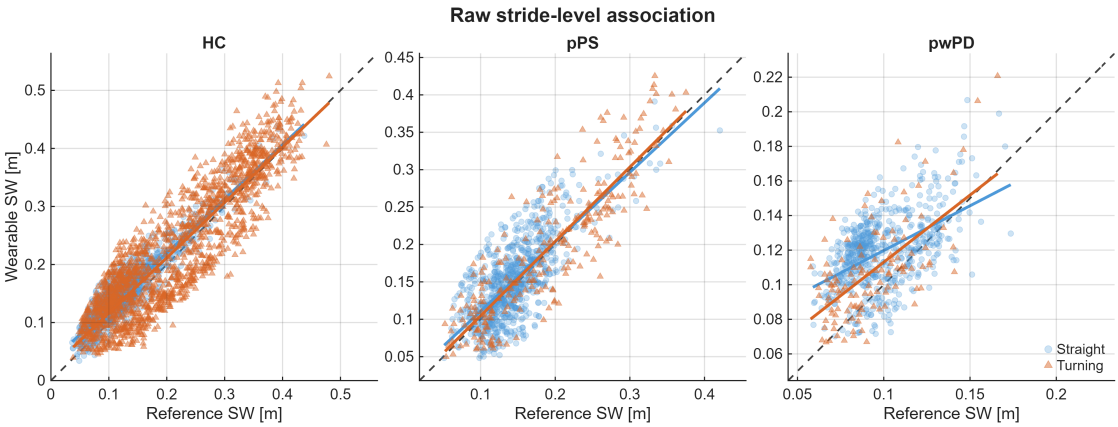



**Figure 4.5:** Raw stride-level association between stereophotogrammetric reference and INDIP stride-width estimates in healthy controls, post-stroke participants, and participants with Parkinson's disease. Straight walking and turning are shown separately within each population. The dashed black line represents the identity line ($y = x$), while the coloured solid lines represent condition-specific linear regression fits. Pearson correlation coefficients and 95% confidence intervals are reported separately for each condition.

## Within-subject centred association

To evaluate the ability of the wearable system to follow stride-to-stride changes within the same participant, the analysis was repeated after subtracting the subject- and condition-specific mean from both the stereophotogrammetric and INDIP measurements (Figure 4.6). Consequently, the centred variables represented deviations from each participant's own mean SW, rather than absolute SW values.

In HCs, a strong within-subject association was retained in both walking conditions. The correlation coefficient was $r = 0.90$ during straight walking (95% CI [0.87–0.92]) and $r = 0.95$ during turning (95% CI [0.93–0.96]).

Similarly, pPSs showed a strong centred association during straight walking, with $r = 0.89$ (95% CI [0.83–0.94]). During turning, the correlation remained

positive but was lower, with $r = 0.72$ (95% CI [0.64–0.78]).

In pwPDs, the centred associations were more moderate than those observed in the other populations. During straight walking, the correlation coefficient was $r = 0.65$ (95% CI [0.45–0.75]), whereas during turning it was $r = 0.71$ (95% CI [0.57–0.82]).

Comparison between the raw and centred analyses showed only small changes in the correlation coefficients for HCs and pPSs. In HCs, the coefficients changed from 0.89 to 0.90 during straight walking and from 0.93 to 0.95 during turning. In pPSs, the corresponding values changed from 0.88 to 0.89 during straight walking and from 0.73 to 0.72 during turning.

A different pattern was observed in pwPDs. During straight walking, the centred coefficient remained similar to the raw coefficient ($r = 0.65$ versus $r = 0.63$). During turning, however, the association increased from $r = 0.51$ in the raw analysis to $r = 0.71$ after centering. Therefore, while the relationship between absolute reference and wearable values was more moderate in pwPDs, particularly during turning, the centred analysis showed that a positive association between within-subject changes was retained.

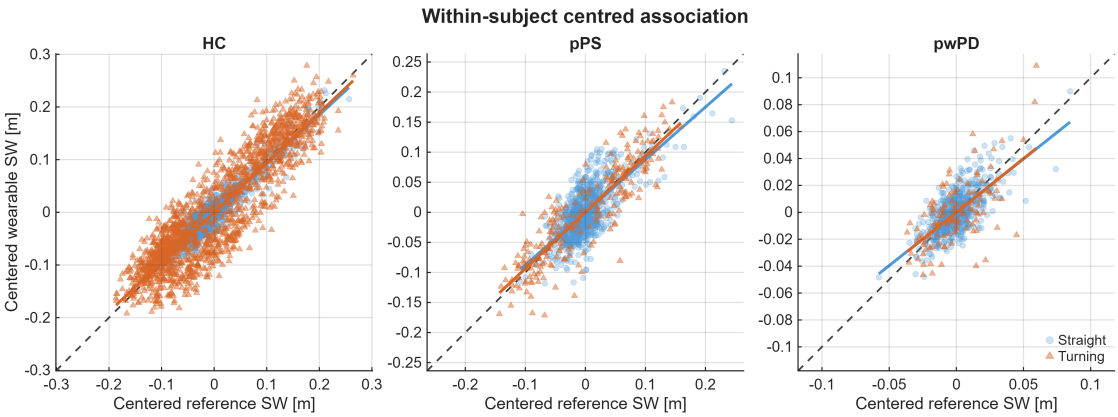



**Figure 4.6:** Within-subject centred association between stereophotogrammetric reference and INDIP stride-width estimates in healthy controls, post-stroke participants, and participants with Parkinson's disease. For each participant and walking condition, the corresponding subject-specific mean was subtracted from both reference and wearable measurements. Straight walking and turning are shown separately. The dashed black line represents the identity line ($y = x$), while coloured solid lines represent condition-specific linear regression fits. Pearson correlation coefficients and 95% confidence intervals are reported for each condition.

## 4.5 Participant-reported acceptability of the wearable system

Participant-reported acceptability of the wearable system was assessed using post-session questionnaires collected within the broader parent-study cohorts from which the participants included in the present validation study were selected. The questionnaire sample therefore did not correspond exactly to the 30 participants included in the stride-width validation dataset, and the acceptability results are reported as complementary information on the usability of the wearable setup.

Three acceptability-related aspects were considered: perceived comfort, perceived safety, and perceived impact on gait. For comfort and safety, the percentage of participants reporting a high rating (VAS $\geq$ 8) was calculated. Perceived gait impact was summarised as the percentage of participants reporting no gait alteration while wearing the system (Figure 4.7).

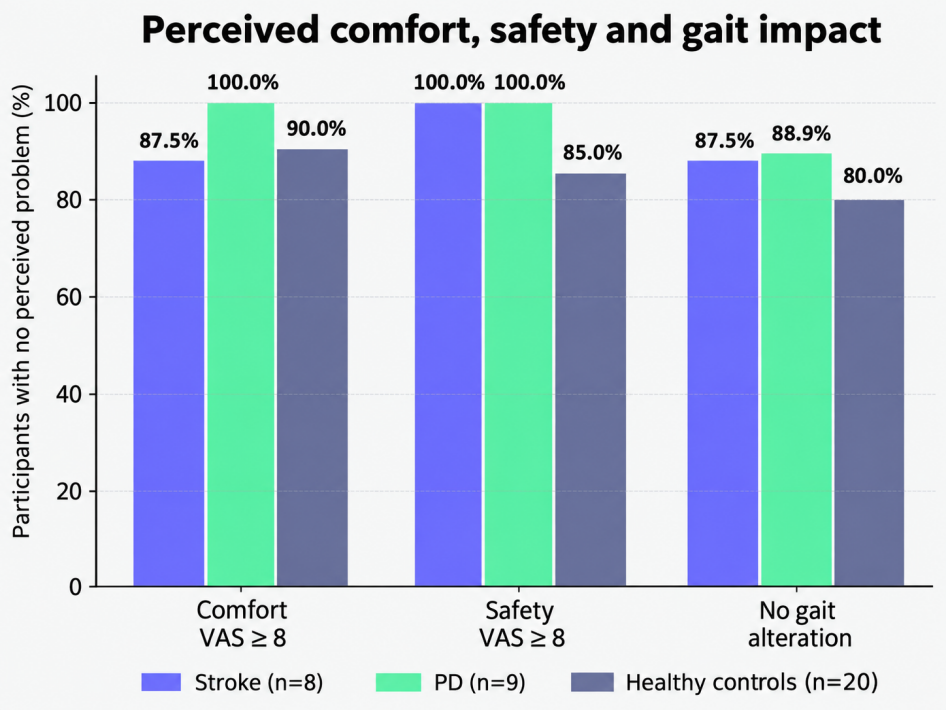



**Figure 4.7:** Participant-reported acceptability of the wearable system among questionnaire respondents. Bars indicate the percentage of participants in each population reporting high comfort (VAS $\geq$ 8), high safety (VAS $\geq$ 8), and no perceived gait alteration while wearing the system. Percentages are calculated within each respondent group: post-stroke ($n = 8$), Parkinson's disease ($n = 9$), and healthy controls ($n = 20$).

Overall, questionnaire responses indicated good acceptability of the wearable system across populations. Among post-stroke respondents ($n = 8$), 87.5% reported high comfort, 100.0% reported high safety, and 87.5% reported no perceived gait alteration. Among respondents with Parkinson's disease ($n = 9$), 100.0% reported high comfort, 100.0% reported high safety, and 88.9% reported no perceived gait alteration. Among healthy controls ($n = 20$), 90.0% reported high comfort, 85.0% reported high safety, and 80.0% reported no perceived gait alteration.

Taken together, these questionnaire findings indicate that, among respondents, the wearable system was generally perceived as comfortable and safe, and was not commonly reported to interfere with gait.

## 4.6 Exploratory analysis of freezing-of-gait-related signal patterns

In addition to the primary SW validation analyses, signals recorded from a participant with Parkinson's disease presenting freezing-of-gait episodes were qualitatively examined to illustrate the complementary information provided by the inertial and inter-foot distance measurements. Representative segments corresponding to standing, regular walking, and a freezing episode were compared.

Figure 4.8 shows the norm of foot acceleration in the three conditions.

During standing, foot acceleration remained close to baseline, with only minimal fluctuations. During regular walking, repeated acceleration peaks were clearly visible, reflecting the cyclic movement of the feet over successive strides. In contrast, the freezing episode was characterised by a markedly less regular signal pattern. Periods containing repeated acceleration bursts alternated with intervals in which foot motion was substantially reduced, resulting in a loss of the regular cyclic pattern observed during walking.

The enlarged portions of the signal further highlight the difference between regular stepping and the altered foot-movement pattern observed during the freezing episode. Whereas regular walking was characterised by recurrent, well-defined acceleration peaks, the freezing segment included temporally irregular bursts and intervals with markedly reduced movement.

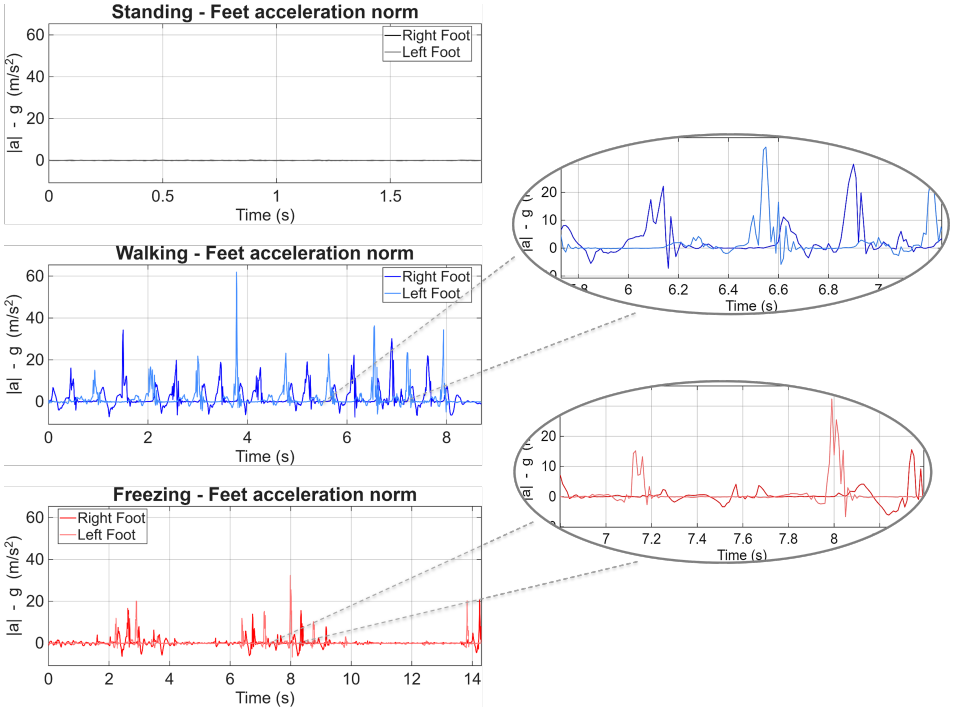



**Figure 4.8:** Representative foot-acceleration signals during standing, regular walking, and a freezing-of-gait episode in a participant with Parkinson's disease. The upper panels show the corresponding reconstructed lower-limb configuration, whereas the lower panels show the norm of foot acceleration over time. Regular walking is characterised by repeated acceleration peaks associated with successive steps, whereas the freezing episode shows a disruption of this regular temporal pattern.

The corresponding inter-foot distance signals are reported in Figure 4.9.

During standing, both the anterior and posterior inter-foot distances remained approximately constant over time. During regular walking, both signals exhibited repeated variations reflecting the cyclic changes in the relative position of the two feet throughout the gait cycle.

During the freezing episode, this regular pattern was disrupted. The inter-foot distance signals showed intervals with reduced variability and relatively stable distances, alternating with periods of larger fluctuations. These temporal changes occurred within the same episode in which the foot-acceleration pattern became irregular, showing that the two sensing modalities provided complementary descriptions of the altered movement.

Taken together, the representative acceleration and inter-foot distance signals showed clearly distinguishable patterns during standing, regular walking, and the selected freezing episode. In particular, the freezing segment was characterised by

a simultaneous disruption of the regular stride-related acceleration pattern and of the cyclic modulation of inter-foot distance.

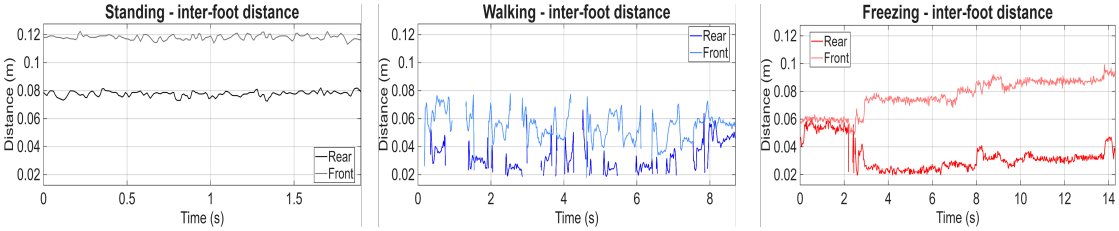



**Figure 4.9:** Representative inter-foot distance signals during standing, regular walking, and a freezing-of-gait episode in a participant with Parkinson's disease. During standing, anterior and posterior inter-foot distances remain approximately stable, whereas regular walking produces repeated stride-related variations. During the freezing episode, the regular temporal modulation is disrupted and intervals with different inter-foot distance patterns can be observed.

# Chapter 5

# Discussion

## 5.1 Validation across populations and walking conditions

The present study extends the validation of the INDIP stride-width estimation method to gait patterns and locomotor conditions that had not been systematically investigated in previous work. The original method proposed by Rossanigo et al. was validated in healthy adults during straight walking at different self-selected speeds, whereas the subsequent methodological development by Cicalò introduced a refined wearable configuration, updated calibration procedures, and the possibility of analysing curvilinear walking. However, validation remained restricted to healthy participants. The main contribution of the present study was therefore to assess whether the same sensing principle could maintain acceptable performance in post-stroke and Parkinsonian gait, where altered motor control, irregular foot placement and different strategies for adapting to locomotor demands may challenge assumptions derived from healthy walking.

This represents a relevant extension of the previous validation framework. Pathological gait does not simply reproduce healthy gait at a different speed. Post-stroke walking may include interlimb asymmetry, compensatory strategies and altered mediolateral regulation of foot placement, while Parkinsonian gait is commonly characterised by reduced movement amplitude, slower progression and impaired adaptation to changing locomotor demands [3,4,6]. These characteristics are particularly relevant for the present wearable approach because stride-width estimation depends on several consecutive processing stages, including gait-event identification, reconstruction of foot motion, acquisition of a valid infrared scan of the contralateral foot and geometrical reconstruction of its footprint. Consequently, an altered gait pattern could potentially affect the final estimate even if the individual sensing components remained technically functional.

Despite these challenges, no systematic increase in absolute stride-width error was observed in either pathological population. Median errors across populations and conditions remained approximately between 1.8 and 4.0 cm, and the pathological groups did not show a general deterioration in performance compared with healthy controls. This finding is particularly relevant because the gait characteristics of the three groups were markedly different. The pwPD group walked substantially more slowly than both HC and pPS and displayed narrower reference stride widths, especially during turning. The pPS group, although closer to HC in terms of walking velocity, represents a heterogeneous population in which asymmetric and compensatory gait strategies are expected [6,17,18]. The fact that these differences were not accompanied by a systematic increase in wearable error suggests that the method is not restricted to a narrowly defined healthy gait pattern.

A direct numerical comparison with the first validation study should nevertheless be made cautiously. Rossanigo et al. reported stride-width RMSE values of approximately 14–18 mm in healthy participants during straight walking [2], whereas the present work reports median absolute errors and includes a different wearable configuration, different processing refinements, turning, and neurological populations. The two error measures are not equivalent and should therefore not be interpreted as evidence of an improvement or deterioration of a specific magnitude. More importantly, the current study addresses a different validation question: rather than confirming performance only under controlled healthy straight walking, it tests whether useful estimation can be preserved over a much broader range of gait behaviours.

Walking condition provided further insight into the limits of the method. Turning is particularly relevant because stride width is defined relative to the local direction of progression, which changes continuously during curvilinear walking. Moreover, the relative position and orientation of the feet change more rapidly than during steady straight walking. This is important for the infrared component of the system, since time-of-flight measurements are sensitive to the geometry of the sensor–target interaction, including relative orientation, incidence angle and target visibility [43]. Errors introduced at this stage propagate to the fitted medial border of the contralateral foot and consequently to the reconstructed footprint used for stride-width estimation.

Consistently with this increased geometrical complexity, turning significantly increased the absolute error in healthy controls. However, the same worsening was not observed in pPS or pwPD. This result should not be interpreted as evidence that pathological turning is intrinsically easier for the wearable system. Instead, the gait-characteristic results indicate that turning was performed differently by the three populations. HC markedly increased their reference stride width during turning, whereas the increase was smaller in pPS and absent in pwPD, who maintained a particularly narrow base of support and walked at markedly lower velocities. This

pattern is compatible with the literature describing turning as a task requiring substantial adaptation of foot placement in healthy walking, while pwPD may adopt shorter steps, reduced turning speed and less effective widening of the base of support [21,22].

The different turning strategies may therefore have exposed the sensing system to different geometrical conditions. In HC, the larger lateral displacement of the feet and the continuous change in direction may have produced a wider range of sensor–foot configurations and consequently more challenging infrared scans. In pwPD, by contrast, slower progression and smaller mediolateral excursions may have resulted in a more spatially constrained sensor–target geometry despite the greater clinical complexity of the movement. This interpretation remains hypothetical, since incidence angle and scan geometry were not directly quantified in the present analysis. Nevertheless, it provides an important indication that measurement difficulty should not be inferred solely from the clinical complexity of the task: the actual kinematics with which the task is performed are also likely to influence wearable performance.

The gait results themselves are also consistent with the clinical characteristics described in the literature. The markedly reduced walking velocity observed in the pwPD group agrees with the well-established hypokinetic gait phenotype of Parkinson's disease [3,4]. In addition, the failure to increase stride width during turning is in line with previous observations that people with Parkinson's disease may have difficulty adapting the base of support to the increased mediolateral demands of directional changes [22]. In contrast, the pPS group showed a clear increase in stride width during turning. This should not be interpreted as evidence of a uniform post-stroke strategy, since post-stroke gait is intrinsically heterogeneous and lateral foot placement can depend on paretic-side impairment, compensation and turning direction [18,19]. However, it confirms that the present validation dataset included substantially different strategies for managing the same locomotor task, further strengthening the relevance of evaluating the wearable method across populations rather than only in healthy participants.

## 5.2 Agreement, within-subject tracking and clinical interpretation

The Bland–Altman analysis highlighted an important distinction between average group-level agreement and individual measurement differences. INDIP showed a positive mean bias relative to stereophotogrammetry in both walking conditions, with average differences of 2.25 cm during straight walking and 1.23 cm during turning. However, the individual subject-level differences were not uniformly small, and the limits of agreement indicated relevant inter-subject variability

in absolute agreement. Thus, considering the mean bias alone would provide an incomplete description of measurement performance, since some participants showed considerably larger differences between INDIP and the reference system than others.

This inter-subject variability is particularly relevant when considering the potential use of the system for longitudinal monitoring. A subject-specific systematic offset may limit the accuracy of comparisons based on absolute stride-width values across different individuals, while having a smaller impact on the ability to detect changes relative to the same individual's usual walking pattern. For this reason, the association between INDIP and stereophotogrammetry was examined not only using the original measurements, but also after removing the subject- and condition-specific mean from both systems.

The within-subject centred analysis therefore addressed a different question from absolute agreement: rather than asking whether INDIP reproduced the exact stride-width value measured by stereophotogrammetry, it assessed whether the wearable system followed stride-to-stride deviations from each participant's own mean behaviour. This distinction is important because a subject-specific offset can affect absolute agreement without necessarily preventing the wearable system from tracking relative changes within that subject.

Several components of the processing pipeline may contribute to this systematic difference. The wearable estimate does not directly measure the position of both heels. Instead, the instrumented foot trajectory is reconstructed from inertial data, the contralateral medial foot border is sampled by two infrared sensors, the detected points are approximated by a linear model, and the full contralateral footprint is then reconstructed using participant-specific geometrical information. Small errors in foot orientation, sensor calibration, distance measurement or medial-border fitting can therefore translate into a displacement of the reconstructed heel point. This differs fundamentally from stereophotogrammetry, where the reference heel position is obtained directly from tracked markers. A small systematic offset in the reconstructed footprint is consequently plausible and could explain why high correlation can coexist with a positive bias.

This consideration is consistent with the original development of the method. Rossanigo et al. already observed that the reconstruction of the non-instrumented foot represented an important source of uncertainty, because its position was inferred from infrared scans rather than directly reconstructed from inertial integration [2]. The present results suggest that this issue remains relevant after extension of the method to more heterogeneous gait patterns. At the same time, the preservation of strong associations in HC and pPS indicates that the resulting reconstruction error does not completely obscure stride-to-stride variability.

The centred correlations remained high in HC and pPS and positive in pwPD. This is particularly informative in the Parkinson's disease group. During turning,

the raw coefficient was $r = 0.51$, whereas after centering it increased to $r = 0.71$. The improvement suggests that the relatively modest raw association was partly influenced by between-subject differences in absolute measurement level. Once these baseline differences were removed, the association between stride-to-stride deviations was stronger. In straight walking the change was much smaller, from $r = 0.63$ to $r = 0.65$, indicating that the relative contribution of between- and within-subject variability differed according to walking condition.

This result is potentially important for the intended role of a wearable gait monitoring system. Laboratory stereophotogrammetry is well suited to obtaining accurate absolute measurements within a controlled session, whereas one of the main advantages of wearable technology is the possibility of collecting repeated measurements over time and in less constrained environments [7,25,26]. In such applications, the ability to detect a deviation from an individual's previous behaviour may be more relevant than the ability to reproduce the exact absolute laboratory value for comparisons between different individuals.

However, the present centred analysis should not be interpreted as direct evidence of longitudinal validity. It evaluates within-subject stride-to-stride covariation during the same experimental dataset; it does not establish test–retest reliability across different days, nor does it demonstrate sensitivity to disease progression or treatment-related change. Rather, it supports the use of within-subject monitoring as a particularly relevant application to be tested in future repeated-session studies.

The $MDC_{95}$ analysis provides complementary information in this respect. For pwPD, the estimated measurement change required to exceed expected measurement variability was approximately 2 cm. This value was close to the 1.82 cm minimally important difference reported by Baudendistel et al. [45] during straight walking. This comparison is clinically interesting, but its interpretation requires caution because MDC and MID address different questions. The MDC is determined by measurement variability and identifies the magnitude of change that is unlikely to be attributable to measurement error alone, whereas the MID represents the magnitude of change considered clinically meaningful.

The fact that the two values are of the same order of magnitude is therefore encouraging, but it does not imply that every clinically relevant change can already be detected reliably. Indeed, the estimated $MDC_{95}$ is slightly larger than the reported MID. Consequently, a change around the published 1.82 cm threshold could potentially fall within the measurement uncertainty of the system. The comparison is also conservative because the available MID refers to straight walking, while measurement uncertainty was investigated in both straight and turning conditions in the present study. No equivalent clinically meaningful threshold was available to interpret turning. These results therefore position the current system close to a potentially useful range of sensitivity, while also indicating that further improvements in repeatability and dedicated longitudinal validation would

be required before clinical change could be interpreted at the individual-patient level.

## 5.3 Practical applicability and additional potential of the wearable system

Measurement validity alone is not sufficient for a wearable system intended for repeated or ecological gait assessment. The sensing setup must also be tolerable and should interfere as little as possible with the movement that is being measured. The acceptability data collected within the broader parent-study cohorts provide useful complementary information in this respect. High comfort and safety ratings were reported by most respondents across populations, and most participants reported no perceived alteration of gait while wearing the system.

These questionnaire results should not be interpreted as an additional validation of measurement accuracy, and the respondents did not correspond exactly to the 30 participants included in the present validation dataset. Moreover, the absence of a *perceived* gait alteration does not demonstrate that the instrumentation had no biomechanical effect. Nevertheless, the results indicate that the wearable configuration was generally well tolerated across both healthy and neurological populations. This is relevant because the current right-foot support combines a MIMU and two ToF sensors and therefore introduces more hardware than a conventional single-IMU setup. Good perceived comfort suggests that this additional sensing information can be obtained without making the system unacceptable to most users.

The multi-sensor nature of INDIP is particularly relevant when considering future applications beyond stride-width estimation. Conventional foot-mounted inertial sensors are effective for reconstructing foot motion and estimating several spatiotemporal gait parameters, but they do not directly measure the position of one foot relative to the other. The infrared sensors address this limitation by providing an independent observation of inter-foot geometry. This additional information may become especially valuable in pathological gait, where clinically relevant alterations may involve not only the timing or amplitude of individual foot movements but also their spatial relationship.

The exploratory FoG example provides an illustration of this potential. In one pwPD, a freezing episode was identified visually from the Vicon recordings and the corresponding temporal interval was annotated. Compared with regular walking, the episode showed disruption of the cyclic acceleration pattern together with marked changes in the inter-foot distance signals. This is consistent with the episodic and heterogeneous nature of FoG described in the literature, which may include progressively shorter shuffling steps, trembling without effective progression, or

transient inability to step [23,24]. Turning is also recognised as one of the locomotor contexts most likely to trigger FoG [5], making the inclusion of curvilinear walking particularly relevant for future wearable monitoring.

The present observation cannot demonstrate automatic FoG detection or classification, since it derives from a single participant and the event was identified using the external Vicon reference rather than by an automated wearable algorithm. Its value is instead conceptual: acceleration and inter-foot distance provide different views of the same movement disturbance. An inertial signal may identify changes in movement intensity and rhythmicity, whereas distance sensing can describe how the spatial relationship between the feet changes during the event. Future algorithms combining these signals could therefore investigate whether this complementarity improves the characterisation of shuffling, trembling or other transient gait disturbances compared with inertial sensing alone.

## 5.4 Strengths, limitations and future developments

A major strength of the present study is the extension of a previously developed wearable method to two neurological populations characterised by substantially different gait impairments. Validation was performed using stride-by-stride matching against stereophotogrammetry and included both straight walking and turning, thereby testing the system under a broader range of locomotor conditions than the original validation. More than 4,500 matched stride-width estimates were retained, allowing the behaviour of the system to be examined over a wide range of individual strides rather than only through a small number of averaged measurements.

Another methodological strength is that the wearable and reference stride-width estimates were based on the same heel-based geometrical definition and on a local direction of progression. This is particularly important during turning, where a fixed laboratory direction would not appropriately describe mediolateral foot placement. Applying the same geometrical definition to both measurement systems therefore reduces the risk that disagreement simply reflects different definitions of stride width rather than measurement error.

At the same time, the number of independent clinical participants remains the main limitation. Only six pPS and six pwPD were included, and turning data were available for only four of the six pwPD. The large number of analysed strides does not compensate for a small number of independent participants, particularly when the objective is to generalise results to heterogeneous neurological populations. The wide confidence intervals observed for some pwPD correlations, especially during turning, reflect this limitation. Population-specific findings should therefore be considered preliminary until replicated in larger cohorts.

Clinical heterogeneity also limits the interpretation of between-subject differences. The pwPD group covered Hoehn and Yahr stages 2–4 and included different levels of walking-aid use, whereas detailed descriptors such as disease severity, paretic side and time since stroke were not available for the pPS dataset. Consequently, it was not possible to determine whether estimation performance varied systematically with clinical severity or with specific post-stroke gait phenotypes. This is particularly relevant in pPS, where asymmetry and compensatory strategies may differ markedly between individuals [17–19].

A further limitation arises from the fact that the datasets originated from different parent studies and acquisition centres. Although the foot-mounted wearable configuration was kept consistent, the groups differed in age, laboratory configuration, walkway length and stereophotogrammetric setup. HC were also considerably younger than the two clinical groups. These differences were an inevitable consequence of combining existing cohorts and allowed access to clinically relevant data, but they prevent population effects from being interpreted as purely disease-related. Future validation should ideally include age-matched controls and more harmonised acquisition protocols.

Calibration also deserves specific consideration. The standard procedure used distance measurements collected during data personalisation, but an alternative marker-based calibration had to be introduced for a subset of clinical acquisitions when those signals were unavailable. This solution prevented the exclusion of otherwise valid data and allowed the same downstream estimation pipeline to be retained. However, because the alternative calibration relies on stereophotogrammetric marker geometry, the wearable estimate is not fully independent from the laboratory reference in those acquisitions. A future out-of-laboratory implementation would therefore require a robust calibration procedure that can be performed entirely with wearable or easily obtainable measurements.

The present study was also conducted in controlled experimental conditions. Although the 2MWT introduced repeated directional changes and continuous walking, it still does not reproduce the full complexity of daily-life mobility. Real-world locomotion includes irregular trajectories, variable surfaces, obstacles, spontaneous speed changes, dual-task conditions and transitions between activities. These factors may affect inertial reconstruction, gait-event detection and the availability and quality of ToF scans. Validation under free-living conditions therefore represents a necessary next step before the system can be considered a tool for ecological stride-width monitoring.

Future work should consequently proceed in two complementary directions. First, the measurement properties of the system should be strengthened through larger clinical samples, age-matched controls and repeated-session protocols. Test–retest studies would allow a more rigorous characterisation of measurement uncertainty

and would directly test whether the encouraging within-subject associations observed here translate into reliable longitudinal tracking. Second, the processing pipeline should be challenged in progressively less constrained walking conditions, with particular attention to automated quality control of ToF scans and to robust calibration without laboratory instrumentation.

Finally, the combination of inertial, pressure and inter-foot distance information offers opportunities beyond the estimation of a single spatial parameter. The exploratory FoG observation suggests that the system may capture complementary features of complex pathological gait events. Dedicated studies could investigate whether these signals improve the recognition or characterisation of turning impairments, shuffling and freezing, while the stride-width estimates themselves could be evaluated as longitudinal markers of changes in balance-control strategy. Such developments would move the system from a laboratory-validated measurement method towards the broader objective that motivated its design: quantitative, repeatable and ecologically meaningful assessment of gait outside conventional motion-analysis laboratories.

# Chapter 6

# Conclusions

This thesis evaluated the validity of the INDIP inertial–infrared wearable system for stride-width estimation in healthy controls, post-stroke participants, and people with Parkinson's disease, considering both straight walking and turning. The study therefore extended previous validation work beyond healthy straight walking to neurological gait patterns and more complex locomotor conditions.

Overall, the wearable system maintained comparable stride-width estimation performance across the three populations. Median absolute errors remained in the order of a few centimetres, approximately 1.8–4.0 cm across population and walking-condition combinations, and no systematic increase in error was observed in the pathological groups. Turning significantly increased the estimation error in healthy controls, whereas no significant worsening was detected in post-stroke participants or people with Parkinson's disease. These results indicate that the presence of pathological gait did not, by itself, prevent the system from providing meaningful stride-width estimates.

The comparison with stereophotogrammetry also showed that the wearable measurements should not be interpreted as fully interchangeable with laboratory reference measurements. INDIP showed a positive mean bias in both walking conditions, together with relevant inter-subject variability in absolute agreement. Nevertheless, positive associations between wearable and reference estimates were observed across all populations. Importantly, after subject-mean centering, the association remained strong in healthy controls and post-stroke participants and was preserved, although more moderately, in people with Parkinson's disease. This suggests that the system may be particularly suitable for monitoring changes relative to an individual's own baseline rather than for reproducing exact absolute laboratory values.

The estimated $MDC_{95}$ in people with Parkinson's disease was of the order of 2 cm. This value was close in magnitude to the 1.82 cm minimally important difference previously reported in the literature during straight walking. Although

this comparison does not establish clinical responsiveness, it suggests that the measurement sensitivity of the system is within a range that may be relevant for longitudinal monitoring and motivates further repeated-session validation.

Additional findings supported the practical applicability of the wearable configuration. Questionnaire data collected within the broader parent-study cohorts indicated generally high perceived comfort and safety and limited perceived interference with gait. Moreover, the exploratory analysis of a visually identified freezing-of-gait episode in one participant with Parkinson's disease showed that foot acceleration and inter-foot distance signals provided complementary information during an altered gait event. Although this observation does not demonstrate automatic freezing detection, it highlights the potential value of combining inertial and distance sensing beyond stride-width estimation.

In conclusion, the present findings support the feasibility of the INDIP system for stride-width assessment across heterogeneous gait patterns and walking conditions. Its main potential appears to lie in repeated, subject-specific gait monitoring, where the ability to capture changes relative to an individual's own walking pattern may be more relevant than exact agreement with a laboratory reference at a single time point. Future studies should confirm these findings in larger clinical cohorts, evaluate test–retest reliability across repeated sessions, and progressively extend validation towards less constrained and real-world walking conditions.

# Bibliography


[1] Veronica Cimolin and Manuela Galli. «Summary measures for clinical gait analysis: A literature review». In: *Gait & posture* 39.4 (2014), pp. 1005–1010 (cit. on p. 1).

[2] Rachele Rossanigo, Marco Caruso, Stefano Bertuletti, Franca Deriu, Marco Knaflitz, Ugo Della Croce, and Andrea Cereatti. «Base of support, step length and stride width estimation during walking using an inertial and infrared wearable system». In: *Sensors* 23.8 (2023), p. 3921 (cit. on pp. 1, 2, 8, 27, 29, 32, 34, 42, 46).

[3] Anat Mirelman et al. «Gait impairments in Parkinson's disease». In: *The Lancet Neurology* 18.7 (2019), pp. 697–708 (cit. on pp. 1, 9, 11).

[4] Ana Paula Janner Zanardi, Edson Soares da Silva, Rochelle Rocha Costa, Elren Passos-Monteiro, Ivan Oliveira Dos Santos, Luiz Fernando Martins Kruel, and Leonardo Alexandre Peyré-Tartaruga. «Gait parameters of Parkinson's disease compared with healthy controls: a systematic review and meta-analysis». In: *Scientific reports* 11.1 (2021), p. 752 (cit. on pp. 1, 11).

[5] Carolina I Conde, Charlotte Lang, Christian R Baumann, Chris A Easthope, William R Taylor, and Deepak K Ravi. «Triggers for freezing of gait in individuals with Parkinson's disease: a systematic review». In: *Frontiers in neurology* 14 (2023), p. 1326300 (cit. on pp. 1, 11).

[6] Dhanya Menoth Mohan, Ahsan Habib Khandoker, Sabahat Asim Wasti, Sarah Ismail Ibrahim Ismail Alali, Herbert F Jelinek, and Kinda Khalaf. «Assessment methods of post-stroke gait: A scoping review of technology-driven approaches to gait characterization and analysis». In: *Frontiers in Neurology* 12 (2021), p. 650024 (cit. on pp. 2, 9, 10).

[7] Francesca Salis et al. «A multi-sensor wearable system for the assessment of diseased gait in real-world conditions». In: *Frontiers in Bioengineering and Biotechnology* 11 (2023), p. 1143248 (cit. on pp. 2, 29, 32).

[8] Giulia Cicalo. «Optimization and validation of a wearable-based method for the ecological estimation of base of support parameters in healthy subjects». PhD thesis. Politecnico di Torino, 2025 (cit. on pp. 3, 30, 32, 33, 38, 40, 42, 46–48).

[9] Jacquelin Perry and Judith M. Burnfield. *Gait Analysis: Normal and Pathological Function*. 2nd ed. SLACK Incorporated, 2010 (cit. on pp. 4–7).

[10] Michael W. Whittle. *Gait Analysis: An Introduction*. 5th ed. Elsevier, 2014 (cit. on pp. 4–7).

[11] Navleen Kour, Sunanda, and Sakshi Arora. «Computer-Vision Based Diagnosis of Parkinson's Disease via Gait: A Survey». In: *IEEE Access* 7 (2019), pp. 156620–156645. DOI: 10.1109/ACCESS.2019.2949744 (cit. on p. 5).

[12] Donald A. Neumann. *Kinesiology of the Musculoskeletal System: Foundations for Rehabilitation*. Mosby Elsevier, 2010 (cit. on p. 6).

[13] Frances Huxham, Jing Gong, Richard Baker, Meg E. Morris, and Robert Iansek. «Defining Spatial Parameters for Non-Linear Walking». In: *Gait & Posture* 23.2 (2006), pp. 159–163. DOI: 10.1016/j.gaitpost.2005.01.001 (cit. on p. 8).

[14] Stacy Fritz and Michelle Lusardi. «White Paper: Walking Speed: The Sixth Vital Sign». In: *Journal of Geriatric Physical Therapy* 32.2 (2009), pp. 46–49. DOI: 10.1519/00139143-200932020-00002 (cit. on p. 8).

[15] Jeffrey M. Hausdorff. «Gait Variability: Methods, Modeling and Meaning». In: *Journal of NeuroEngineering and Rehabilitation* 2 (2005), p. 19. DOI: 10.1186/1743-0003-2-19 (cit. on p. 8).

[16] Jennifer S. Brach, Jaime E. Berlin, Jessie M. VanSwearingen, Anne B. Newman, and Stephanie A. Studenski. «Too Much or Too Little Step Width Variability Is Associated with a Fall History in Older Persons Who Walk at or near Normal Gait Speed». In: *Journal of NeuroEngineering and Rehabilitation* 2 (2005), p. 21. DOI: 10.1186/1743-0003-2-21 (cit. on p. 8).

[17] Kara K. Patterson, William H. Gage, Dina Brooks, Sandra E. Black, and William E. McIlroy. «Evaluation of Gait Symmetry after Stroke: A Comparison of Current Methods and Recommendations for Standardization». In: *Gait & Posture* 31.2 (2010), pp. 241–246. DOI: 10.1016/j.gaitpost.2009.10.014 (cit. on pp. 8, 10).

[18] Katy H. Stimpson, Lauren N. Heitkamp, Aaron E. Embry, and Jesse C. Dean. «Post-stroke Deficits in the Step-by-Step Control of Paretic Step Width». In: *Gait & Posture* 70 (2019), pp. 136–140. DOI: 10.1016/j.gaitpost.2019.03.003 (cit. on p. 10).

[19] Rémi Pierre-Marie Barrois, Damien Ricard, Laurent Oudre, Leila Tlili, Clément Provost, Aliénor Vienne, Pierre-Paul Vidal, Stéphane Buffat, and Alain P. Yelnik. «Observational Study of 180-Degree Turning Strategies Using Inertial Measurement Units and Fall Risk in Poststroke Hemiparetic Patients». In: *Frontiers in Neurology* 8 (2017), p. 194. DOI: 10.3389/fneur.2017.00194 (cit. on p. 10).

[20] Meg E. Morris, Robert Iansek, Thomas A. Matyas, and Jeffrey J. Summers. «Stride Length Regulation in Parkinson's Disease: Normalization Strategies and Underlying Mechanisms». In: *Brain* 119.2 (1996), pp. 551–568. DOI: 10.1093/brain/119.2.551 (cit. on p. 11).

[21] Paolo Crenna, Ilaria Carpinella, Marco Rabuffetti, Elena Calabrese, Paolo Mazzoleni, Roberto Nemni, and Maurizio Ferrarin. «The Association between Impaired Turning and Normal Straight Walking in Parkinson's Disease». In: *Gait & Posture* 26.2 (2007), pp. 172–178. DOI: 10.1016/j.gaitpost.2007.04.010 (cit. on p. 11).

[22] Sabato Mellone, Martina Mancini, Laurie A. King, Fay B. Horak, and Lorenzo Chiari. «The Quality of Turning in Parkinson's Disease: A Compensatory Strategy to Prevent Postural Instability?» In: *Journal of NeuroEngineering and Rehabilitation* 13 (2016), p. 39. DOI: 10.1186/s12984-016-0147-4 (cit. on p. 11).

[23] John G. Nutt, Bastiaan R. Bloem, Nir Giladi, Mark Hallett, Fay B. Horak, and Alice Nieuwboer. «Freezing of Gait: Moving Forward on a Mysterious Clinical Phenomenon». In: *The Lancet Neurology* 10.8 (2011), pp. 734–744. DOI: 10.1016/S1474-4422(11)70143-0 (cit. on pp. 11, 12).

[24] Joanna D. Schaafsma, Yacov Balash, Tanya Gurevich, Anna L. Bartels, Jeffrey M. Hausdorff, and Nir Giladi. «Characterization of Freezing of Gait Subtypes and the Response of Each to Levodopa in Parkinson's Disease». In: *European Journal of Neurology* 10.4 (2003), pp. 391–398. DOI: 10.1046/j.1468-1331.2003.00611.x (cit. on p. 11).

[25] Alvaro Muro-de-la-Herran, Begonya Garcia-Zapirain, and Amaia Mendez-Zorrilla. «Gait Analysis Methods: An Overview of Wearable and Non-Wearable Systems, Highlighting Clinical Applications». In: *Sensors* 14.2 (2014), pp. 3362–3394. DOI: 10.3390/s140203362 (cit. on pp. 12, 18).

[26] Weijun Tao, Tao Liu, Rencheng Zheng, and Hutian Feng. «Gait Analysis Using Wearable Sensors». In: *Sensors* 12.2 (2012), pp. 2255–2283. DOI: 10.3390/s120202255 (cit. on pp. 12, 18, 24).

[27] Aurelio Cappozzo, Ugo Della Croce, Alberto Leardini, and Lorenzo Chiari. «Human Movement Analysis Using Stereophotogrammetry. Part 1: Theoretical Background». In: *Gait & Posture* 21.2 (2005), pp. 186–196. DOI: 10.1016/j.gaitpost.2004.01.010 (cit. on pp. 13, 15, 16).

[28] Lorenzo Chiari, Ugo Della Croce, Alberto Leardini, and Aurelio Cappozzo. «Human Movement Analysis Using Stereophotogrammetry. Part 2: Instrumental Errors». In: *Gait & Posture* 21.2 (2005), pp. 197–211. DOI: 10.1016/j.gaitpost.2004.04.004 (cit. on pp. 14, 16, 17).

[29] Aurelio Cappozzo, Fabio Catani, Ugo Della Croce, and Alberto Leardini. «Position and Orientation in Space of Bones during Movement: Anatomical Frame Definition and Determination». In: *Clinical Biomechanics* 10.4 (1995), pp. 171–178. DOI: 10.1016/0268-0033(95)91394-T (cit. on p. 15).

[30] Ugo Della Croce, Alberto Leardini, Lorenzo Chiari, and Aurelio Cappozzo. «Human Movement Analysis Using Stereophotogrammetry. Part 4: Assessment of Anatomical Landmark Misplacement and Its Effects on Joint Kinematics». In: *Gait & Posture* 21.2 (2005), pp. 226–237. DOI: 10.1016/j.gaitpost.2004.05.003 (cit. on p. 17).

[31] Ugo Della Croce, Aurelio Cappozzo, and D. Casey Kerrigan. «Pelvis and Lower Limb Anatomical Landmark Calibration Precision and Its Propagation to Bone Geometry and Joint Angles». In: *Medical & Biological Engineering & Computing* 37 (1999), pp. 155–161. DOI: 10.1007/BF02513282 (cit. on p. 17).

[32] Alberto Leardini, Lorenzo Chiari, Ugo Della Croce, and Aurelio Cappozzo. «Human Movement Analysis Using Stereophotogrammetry. Part 3: Soft Tissue Artifact Assessment and Compensation». In: *Gait & Posture* 21.2 (2005), pp. 212–225. DOI: 10.1016/j.gaitpost.2004.05.002 (cit. on p. 17).

[33] Daniel Roetenberg, Henk J. Luinge, Chris T. M. Baten, and Peter H. Veltink. «Compensation of Magnetic Disturbances Improves Inertial and Magnetic Sensing of Human Body Segment Orientation». In: *IEEE Transactions on Neural Systems and Rehabilitation Engineering* 13.3 (2005), pp. 395–405. DOI: 10.1109/TNSRE.2005.847353 (cit. on pp. 18, 22, 23).

[34] Sebastian O. H. Madgwick, Andrew J. L. Harrison, and Ravi Vaidyanathan. «Estimation of IMU and MARG Orientation Using a Gradient Descent Algorithm». In: *2011 IEEE International Conference on Rehabilitation Robotics*. 2011, pp. 1–7. DOI: 10.1109/ICORR.2011.5975346 (cit. on pp. 18, 21, 23, 24).

[35] Angelo Maria Sabatini. «Quaternion-Based Strap-Down Integration Method for Applications of Inertial Sensing to Gait Analysis». In: *Medical & Biological Engineering & Computing* 43.1 (2005), pp. 94–101. DOI: 10.1007/BF02345128 (cit. on p. 21).

[36] T. R. McGuire and R. I. Potter. «Anisotropic Magnetoresistance in Ferromagnetic 3d Alloys». In: *IEEE Transactions on Magnetics* 11.4 (1975), pp. 1018–1038. DOI: 10.1109/TMAG.1975.1058782 (cit. on p. 22).

[37] Franco Ferraris, Ugo Grimaldi, and Marco Parvis. «Procedure for Effortless In-Field Calibration of Three-Axis Rate Gyros and Accelerometers». In: *Sensors and Materials* 7.5 (1995), pp. 311–330 (cit. on p. 23).

[38] David Tedaldi, Alberto Pretto, and Emanuele Menegatti. «A Robust and Easy to Implement Method for IMU Calibration without External Equipments». In: *2014 IEEE International Conference on Robotics and Automation*. 2014, pp. 3042–3049. DOI: 10.1109/ICRA.2014.6907297 (cit. on p. 23).

[39] Diana Trojaniello, Andrea Cereatti, Elisa Pelosin, Laura Avanzino, Anat Mirelman, Jeffrey M. Hausdorff, and Ugo Della Croce. «Estimation of Step-by-Step Spatio-Temporal Parameters of Normal and Impaired Gait Using Shank-Mounted Magneto-Inertial Sensors: Application to Elderly, Hemiparetic, Parkinsonian and Choreic Gait». In: *Journal of NeuroEngineering and Rehabilitation* 11 (2014), p. 152. DOI: 10.1186/1743-0003-11-152 (cit. on pp. 24, 25).

[40] Angelo M. Sabatini, Chiara Martelloni, Sergio Scapellato, and Filippo Cavallo. «Assessment of Walking Features from Foot Inertial Sensing». In: *IEEE Transactions on Biomedical Engineering* 52.3 (2005), pp. 486–494. DOI: 10.1109/TBME.2004.840727 (cit. on p. 25).

[41] Benoit Mariani, Christophe Hoskovec, Stephane Rochat, Christophe Büla, Julien Penders, and Kamiar Aminian. «3D Gait Assessment in Young and Elderly Subjects Using Foot-Worn Inertial Sensors». In: *Journal of Biomechanics* 43.15 (2010), pp. 2999–3006. DOI: 10.1016/j.jbiomech.2010.07.003 (cit. on p. 25).

[42] Francesca Salis, Stefano Bertuletti, Tecla Bonci, Ugo Della Croce, Claudia Mazzà, and Andrea Cereatti. «A Method for Gait Events Detection Based on Low Spatial Resolution Pressure Insoles Data». In: *Journal of Biomechanics* 127 (2021), p. 110687. DOI: 10.1016/j.jbiomech.2021.110687 (cit. on pp. 25, 26).

[43] Stefano Bertuletti, Andrea Cereatti, Daniele Comotti, Michele Caldara, and Ugo Della Croce. «Static and Dynamic Accuracy of an Innovative Miniaturized Wearable Platform for Short Range Distance Measurements for Human Movement Applications». In: *Sensors* 17.7 (2017), p. 1492. DOI: 10.3390/s17071492 (cit. on pp. 27, 28).

[44] Stefano Bertuletti, Ugo Della Croce, and Andrea Cereatti. «A Wearable Solution for Accurate Step Detection Based on the Direct Measurement of the Inter-Foot Distance». In: *Journal of Biomechanics* 84 (2019), pp. 274–277. DOI: 10.1016/j.jbiomech.2018.12.039 (cit. on p. 29).

[45] Sidney T. Baudendistel, Allison M. Haussler, Kerri S. Rawson, and Gammon M. Earhart. «Minimal clinically important differences of spatiotemporal gait variables in Parkinson disease». In: *Gait & Posture* 108 (2024), pp. 257–263. DOI: 10.1016/j.gaitpost.2023.11.016 (cit. on p. 59).